ALMA MATER STUDIORUM
UNIVERSITÀ DI BOLOGNA

DOTTORATO DI RICERCA IN

MECCANICA E SCIENZE AVANZATE DELL'INGEGNERIA

Ciclo XXXVII

Settore Concorsuale: 09/C2

Settore Scientifico Disciplinare: ING-IND/18

"*SCALE-UP OF COLD ATMOSPHERIC PLASMA (CAP) SOURCE FOR THE PRODUCTION OF PLASMA ACTIVATED WATER (PAW)*"

Presentata da: ***Roberto Montalbetti***

Coordinatore Dottorato:

Prof. Lorenzo Donati

Supervisore:

Prof. Romolo Laurita

Esame finale anno 2025

ABSTRACT

This thesis explores the scale-up of cold atmospheric plasma (CAP) sources for producing plasma-activated water (PAW), valued for its unique chemical properties derived from reactive oxygen and nitrogen species (RONS). RONS contributes to PAW's antimicrobial and oxidative properties, making it valuable in agriculture, healthcare, and environmental remediation. However, efficient large-scale PAW production remains challenging due to declining CAP efficiency with increasing water volumes. The work begins with a systematic review (submitted to *Plasma Processes and Polymers*) that examines current PAW production methods, analyzing CAP configurations and process variables such as RONS concentration, pH, and energy efficiency. The review highlights various CAP sources, including corona discharge, dielectric barrier discharge (DBD), and plasma jets, examining how parameters like gas type and water composition affect PAW chemistry. Critical challenges for scaling up have also been identified, especially in sustaining high RONS concentrations in larger treatment volumes. Experimental research progresses from a 0.5-liter corona discharge system to a 2-liter DBD setup, increasing the treatment volume fourfold while maintaining RONS concentrations and improving energy efficiency. The research scales PAW production to a 6-liter treatment volume using a multipin corona discharge. This setup addresses challenges such as plasma uniformity and water homogeneity through strategic source placement and mechanical stirring, providing a scalable solution ideal for applications needing large PAW quantities, like agricultural irrigation and soil treatment. Finally, a hybrid CAP source was developed to enhance RONS production further. The optimized design and configuration allowed for greater control over RONS production and improved energy utilization, leading to higher RONS concentrations in treated water than multipin corona. This thesis presents critical insights into parameters for efficient RONS production in large-scale treatments, effectively bridging laboratory results with industrial applications. These findings lay the groundwork for advancing PAW technology, establishing benchmarks for scaling plasma-water treatments across diverse industries.

Index

1. Introduction and aim

This thesis focuses on the scale-up of cold atmospheric plasma (CAP) sources used to puce Plasma Activated Water (PAW). Plasma Activated Water, a product of the interaction between CAP and water, is gaining increasing attention due to its unique chemical and biological properties. These properties are primarily attributed to the generation of Reactive Oxygen and Nitrogen Species (RONS), which are responsible for the antimicrobial, oxidative, and chemical effects of PAW. As such, PAW has found applications in a wide range of fields, including agriculture, healthcare, and environmental decontamination. However, despite its promising potential, the large-scale production of PAW remains a challenge due to the limited efficiency of plasma sources when treating significant water volumes. Therefore, this thesis aims to address this challenge by focusing on the scale-up of plasma sources for industrial-level PAW production.

The thesis begins with a systematic review published in the journal '*Plasma Processes and Polymers*' [63], which serves as the introductory section of this work. The review provides a detailed analysis of the existing literature on PAW production, examining the different methodologies used to produce PAW and the role of CAP process parameters in determining the concentration of RONS and other critical factors, such as pH and energy efficiency. The review systematically categorizes the various plasma sources, including corona discharge, Dielectric Barrier Discharge (DBD), and plasma jets, as well as the different gases used in these processes. By reprocessing the data from the literature, the review highlights how the different plasma-water configurations impact RONS production and identifies the key challenges associated with scaling up these processes for practical applications. Following the review, the thesis presents experimental work aimed at scaling up PAW production from laboratory settings to more practical, larger-scale processes.

The initial experimental setup involves a corona discharge source designed to treat 0.5 liters of water; a configuration commonly used in many laboratory experiments. This section provides a detailed description of the corona discharge setup, including its working mechanism, energy input, and the resulting concentrations of RONS in the treated water. Despite its effectiveness at producing high RONS concentrations, this system is inherently limited by its low treatment volume, which restricts its applicability in industrial scenarios requiring large amounts of treated water.

Building on the insights gained from the corona discharge experiments, the thesis then introduces the development of a Dielectric Barrier Discharge (DBD) system capable of treating 2 liters of water. This represents a significant step forward in the scale-up process, as it quadruples the treatment volume while maintaining high RONS concentrations. The chapter dedicated to the DBD source discusses its technical design, which includes modifications to ensure uniform plasma exposure across the larger water volume and provides comparative data between the corona and DBD sources. The results of these experiments demonstrate that the DBD system not only scales up the treatment volume but also improves the energy efficiency of the process, making it a more viable option for industrial applications.

The final part of the experimental section focuses on further scaling the PAW production system to treat up to 6 liters of water using a dual corona discharge setup. This section delves into the technical challenges encountered during the scale-up process, including the need for optimized plasma source configurations and the use of mechanical stirring to ensure homogeneity in the treated water. By employing two corona discharge sources in a symmetrical configuration, the system achieves uniform plasma generation over the entire water surface, resulting in consistent RONS distribution throughout the treated water volume. This configuration is particularly relevant for applications in agriculture, where large quantities of PAW are needed to ensure the effective treatment of crops orsoil.

In summary, this thesis presents a comprehensive approach to the scale-up of PAW production, beginning with a review of existing literature and culminating in the development and optimization of larger plasma systems. The work addresses key challenges related to the scalability of plasma-water interactions and demonstrates that, with proper design and process optimization, it is possible to maintain high RONS concentrations while treating larger water volumes. By bridging the gap between laboratory-scale experiments and industrial applications, this thesis lays the groundwork for further advancements in the production of PAW and its use in various industries.

2. "Production and chemical composition of Plasma Activated Water: a systematic review and meta-analysis"

Roberto Montalbetti[1], Zdenko Machala[2], Matteo Gherardi[1,3], Romolo Laurita[1,4*]

1 Department of Industrial Engineering, Alma Mater Studiorum - University of Bologna, Bologna, Bologna, Italy

2 Division of Environmental Physics, Faculty of Mathematics, Physics and Informatics, Comenius University Bratislava, Mlynska dolina, Bratislava, Slovakia

3 Interdepartmental Centre for Industrial Research Advanced Mechanical Engineering Applications and Materials Technology, Alma Mater Studiorum - University of Bologna, Bologna, Italy

4 Interdepartmental Centre for Industrial Research Health Sciences and Technologies, Alma Mater Studiorum - University of Bologna, Ozzano dell'Emilia, Bologna, Italy

Abstract: The physio-chemical interplay between Cold atmospheric plasma (CAP) and water confers unique chemical and biological properties to the liquid, producing plasma-activated water (PAW). This review systematically examines various methodologies for PAW production, focusing on the effects of process parameters on Reactive Oxygen and Nitrogen Species (RONS) concentration and pH levels in PAW. It presents detailed analyses of CAP sources, working gases, and treatment conditions, showcasing their impact on PAW processes. The extracted data are reprocessed to derive parameters such as mean energy density and RONS production efficiency. Specific plasma-water configurations exhibit notably higher production rates, indicating promising opportunities for advancing PAW generation techniques and enhancing its applicability in various fields.

Keywords: Cold atmospheric plasma (CAP), Plasma activated water (PAW), Reactive Oxygen and Nitrogen Species (RONS), CAP sources, PAW chemistry.

2.1 Introduction

The production and use of plasma-activated water (PAW) is a pivotal topic in plasma science and technology. The interaction between cold atmospheric plasma (CAP) and water modifies the liquid chemical properties through the production of Reactive Oxygen and Nitrogen Species (RONS) [1–9]. Even if the mechanisms behind the RONS production in PAW involve complex interactions between plasma and water, leading to the formation of both short-lived and long-lived reactive species, the scientific community generally classify dissolved RONS into two macro groups: long-lived species such as hydrogen peroxide (H_2O_2), nitrites (NO_2^-), nitrates (NO_3^-), ozone (O_3), and short-lived species such as hydroxyl radicals ($OH^\cdot$), nitric oxide (NO), superoxide (O_2^-), and peroxinitrous acid (ONOOH). The mechanisms of their formation, chemical reactions, and transport can be found in detail in[1,10–13]. The RONS endow PAW with unique biological properties [14–17], making it efficacious not only in medical treatments such as wound healing and cancer treatment [18–27], but

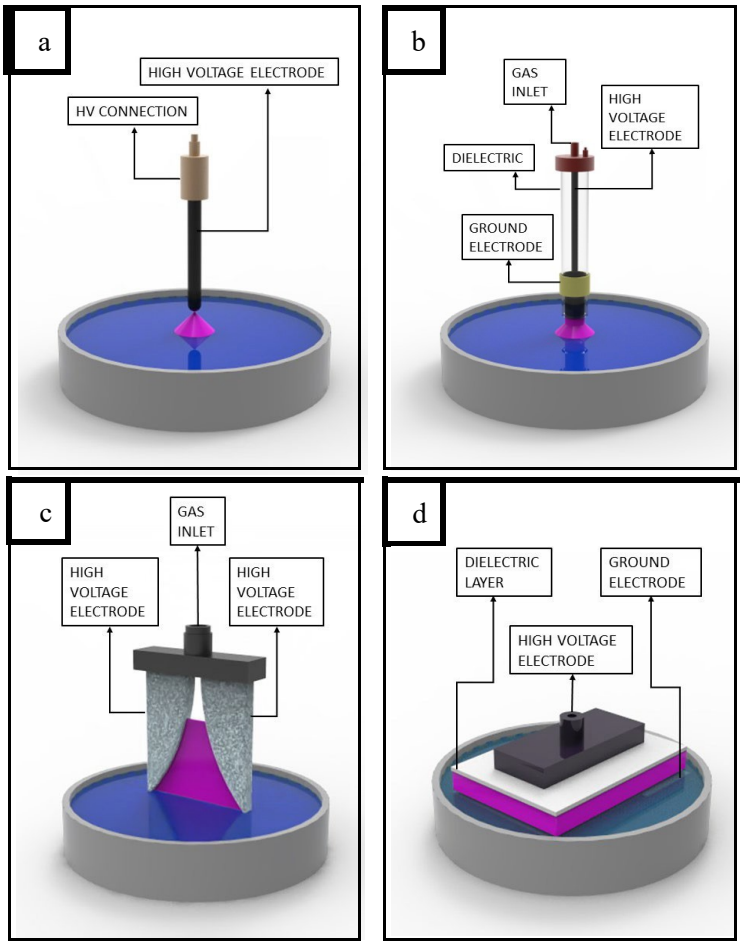

Figure. 1: Plasma-source for PAW treatment. Fig. 1a: Corona Source. Fig. 1b: Plasma-jet source. Fig 1c: Gliding arc source. Fig 1d: Dielectric Barrier Discharge source.

also in agriculture processes, from seed germination to crop protection [28–35]. Additionally, PAW is effective in food processing, significantly enhancing food safety and extending product shelf life [36–43]. Moreover, scientific literature describes the use of PAW in materials processing, materials synthesis, and analytical chemistry [44–49]. The growing interest in PAW has propelled the innovation of new CAP-water processes capable of treating large volumes producing high concentrations of dissolved RONS. Each process parameter of PAW production, including CAP sources (Figure 1), working gas, treated liquid and volume, treatment time, and type of the power supply, specifically affects the treatment outcomes, such as discharge power, RONS concentrations, and pH values. Despite the growing interest of the scientific community, several facets related to PAW still necessitate more comprehensive studies. The chemical-physical interplay between plasma and water and how process parameters affect the pH level and concentration of dissolved RONS still require deeper investigation. This systematic review aims to provide an overview of the different CAP sources above liquid and process parameters reported in the literature to produce PAW and to investigate how the process parameters influence the induced chemistry in liquid. The meta-analysis focuses on the mean energy density of the plasma-water treatment [kWh/l] and the RONS production efficiency [mol/kWh].

2.2 METHODOLOGY

2.2.1 Review Strategy

This report was prepared following the PRISMA 2020 checklist and the guidelines outlined in the PRISMA statement include explanations and elaborations [50]. The Identification process (Figure 2) for relevant papers begins with searches in the online Scopus and Web of Science (WOS) databases. The period starts at the beginning of 2017 and ends at the end of 2023; all papers published before or after this period were not considered. The selected keywords were "plasma-activated water" OR "plasma activated water" OR "plasma-treated water" OR "plasma treated water" OR “Plasma-functionalized water” OR “Plasma functionalized water”. The search included papers and reviews, but the latter were not analyzed in this study.

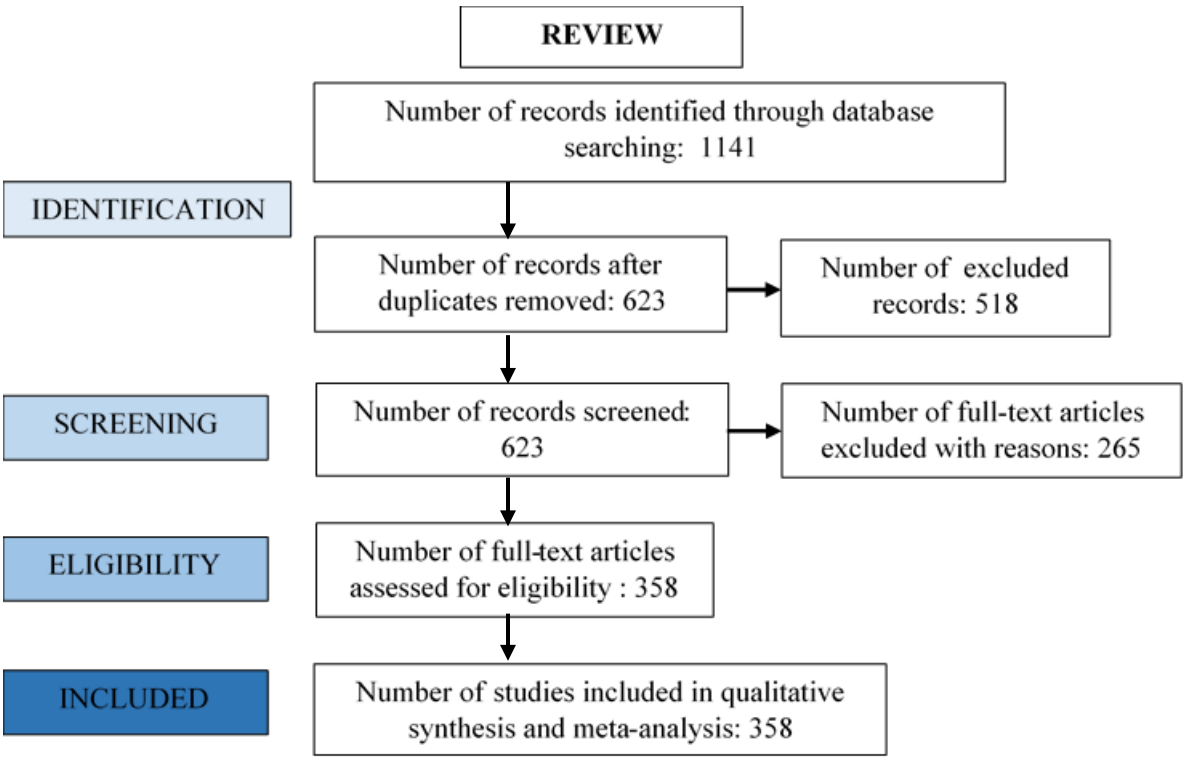

Figure 2: Review strategy summary.

2.2.2 Inclusion and exclusion criteria

Papers included in the analysis must fulfill the following specific criteria:

- The record must report PAW treatment process parameters, including treated water, working gas and flow rate, CAP source, applied voltage, frequency, current, and power supply.
- The record must contain at least two data related to: treated water and volume, working gas and flow rate, CAP source, and treatment time.
- The record must present at least two of the following results: H_2O_2 concentration, NO_2^- concentration, NO_3^- concentration, pH, and power discharge.

All records that did not meet the criteria were discarded. In addition, in the case of papers reporting more than one PAW treatment, only one was selected according to the following inclusion criteria:

- If the record reports multiple experiments based on the following criteria: working gas and gas flow rate, treatment time, and discharge power, the experiment resulting in the highest concentrations of RONS was selected.
- If the record reports multiple experiments based on the treated liquid, the experiment with tap water treatment was selected.
- If the record reports a variation of two or more of the previously mentioned experiment variables, the experiment involving air or tap water was selected (with a bias towards those with the highest concentrations of RONS).

CAP sources are classified as follows:

- Corona Discharge: Utilizes sharp high voltage electrodes [51]. This includes variants such as corona multi-pin, corona pin-to-plate, streamers and streamer-to-spark transition discharges [13,52].
- DBD (Dielectric Barrier Discharge): Involves a high voltage and a grounded electrode with at least one dielectric layer in the interelectrode gap [53].

- Plasma Jet: Features a high voltage wire electrode placed inside a dielectric tube with a working gas flowing through it [54].
- sDBD (surface Dielectric Barrier discharge): Comprises a high voltage electrode positioned on a dielectric surface with a corresponding grounded electrode on the reverse side of the dielectric material[55].
- Gliding Arc: Composed of two tilted electrodes, with or without dielectric material, and a working gas flowing through the electrodes [56].

Microsoft Excel is used to create a database to assess the meta-analysis. Upon completing the Inclusion process, about 4000 data were processed for meta-analysis.

2.3 Results

2.3.1 Literature overview

The geographical and temporal distribution of the screened papers were analysed. Figure 3 describes the number of papers and reviews published between 2017 and 2023. Despite the moderate initial number of publications in the first two years, there is a remarkable increase between 2020 and 2023. This underlined the extending prominence of PAW processes and led to the global expansion of PAW-related papers (as illustrated in Figure 4). The Asian continent is predominant (total 48%; China 22%, India 5% and Japan 3%). Europe emerges as the second most significant region in terms of contributors (total 29%; Italy 6%, Slovakia 5%, Germany 3%), followed by America (total 12%; U.S.A 8% and Canada 3%), and Oceania (total 10%; 6% Australia).

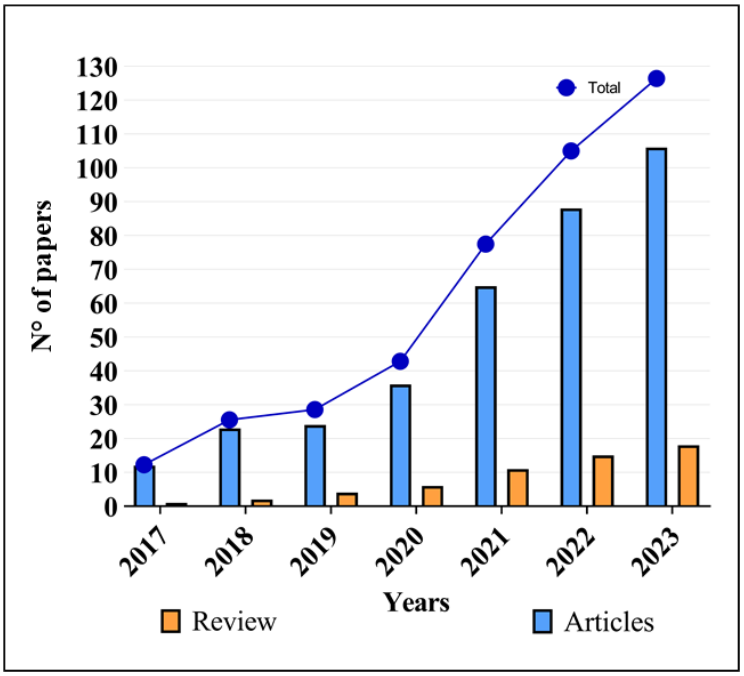

Figure 3: Yearly distribution of the screened papers.

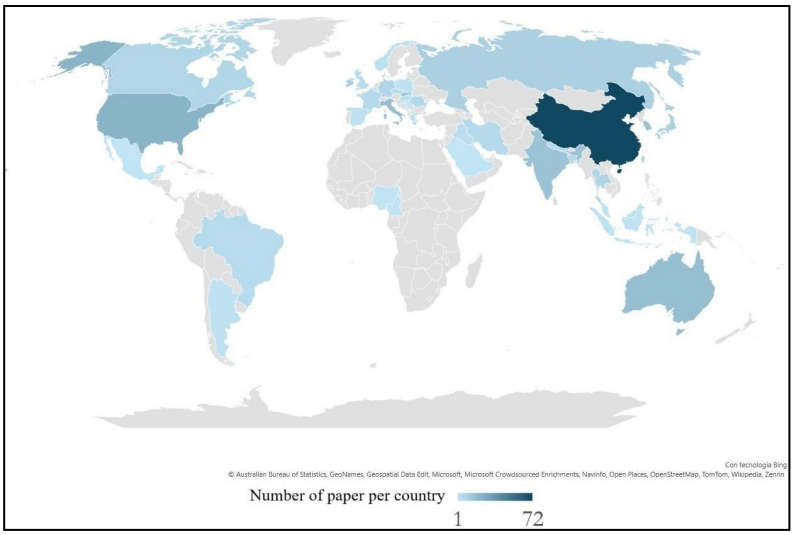

Figure 4: Geographic distribution of the screened papers.

2.3.2 Methods for the production of PAW.

The following charts (Figure 5,6,7) report the annual number of papers published between 2017 and 2023, classified by the CAP source, working gas, and typology of the power supply used for PAW production.

Figure 5 depicts the CAP sources most widely used over the years. The most utilized is the plasma-jet (47%), succeeded by the DBD at 24% and the corona discharge at 16%. CAP sources such as gliding arc and sDBD each contribute 7%.

Figure 6 reports the most employed working gas for PAW production, with air being prevalent (65%), despite biases induced by the inclusion criteria influencing this preference. Other frequently used gases are Ar (14%), and N_2 (6%), He (5%). Mixtures of different gases (e.g. Ar + O_2, O_2 + N_2, He + Air) are used and were classified as 'Other' (6%).

Figure 7 presents the typologies of power supplies used for CAP generation. Sinusoidal voltage (in kHz frequency range) and microsecond or nanosecond pulsed voltages are the most commonly utilized waveforms generated by power supplies, accounting for 44% and 39%, respectively. Other power supplies produce waveforms such as microwave (4%), bi-polar (5%), and radiofrequency (7%).

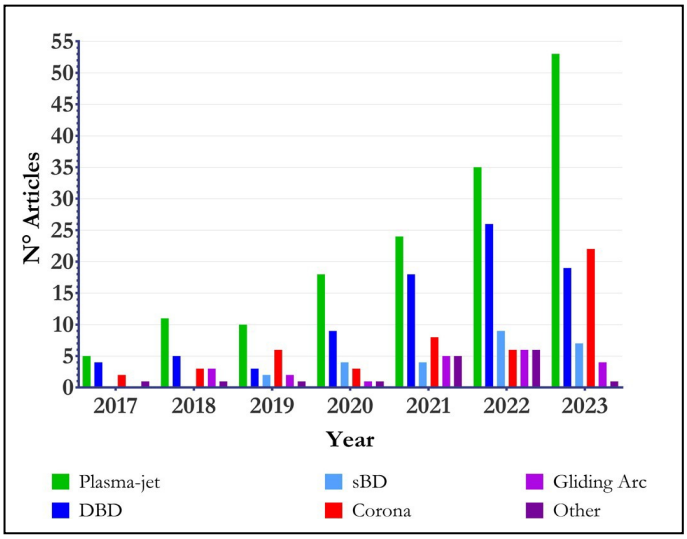

Figure 5: Yearly distribution of CAP sources used for PAW production.

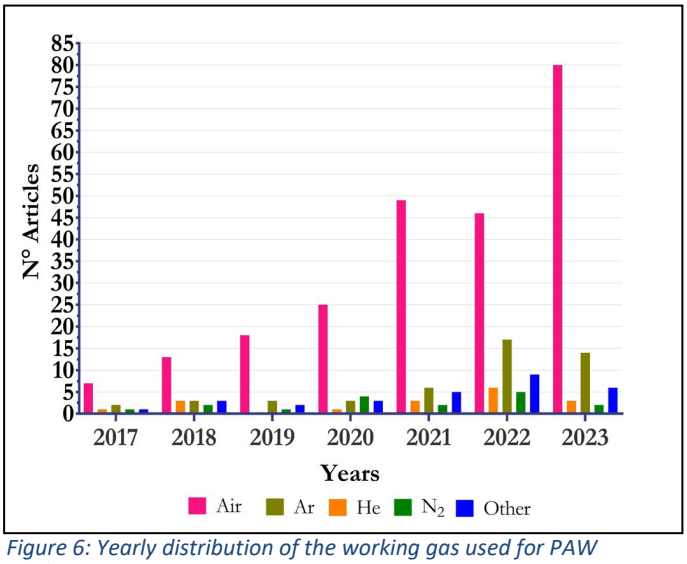

Figure 6: Yearly distribution of the working gas used for PAW production.

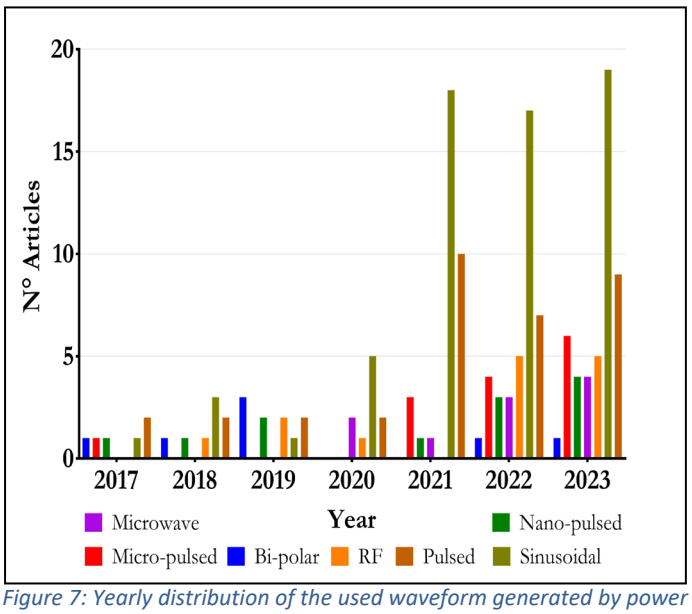

Figure 7: Yearly distribution of the used waveform generated by power supply used for PAW production.

2.3.3 Influence of the type of water and plasma source on RONS concentration.

PAW production involves various types of water derived through different chemical and physical procedures such as distillation, deionization, tap water production, and reverse osmosis. Deionized water is the most commonly used, accounting for 40% of the total, followed by distilled water 34%. Recent years exhibit an increase in tap water use, constituting 10% of the liquids used in PAW processes. Other types of treated water, such as ultrapure water (7%) and reverse osmosis water (2%), are also employed in PAW production. Figures 8,9 and 10 illustrate the concentrations of the most typical long-lived RONS (H_2O_2, NO_2^-, NO_3^-) produced in PAW by treating different types of water using various CAP sources. To emphasize the difference between buffered and non-buffered liquids, water types are classified as pure (including distilled water, de-ionized water, ultrapure water, reverse osmosis water) and tap water. The plasma sources depicted are plasma jets, DBDs, and corona discharges (excluding gliding arc due to a lack of data). In figure 11, the median of the concentration of long lived RONS are reported. The analysis of H_2O_2 concentrations (Figure 11) indicates that plasma jets can produce the highest median concentrations either in pure or tap water, succeeded by DBDs and corona discharges. Pure water results in significantly higher H_2O_2 median concentrations than tap water, regardless the CAP source utilized within the treatment. Regarding NO_2^- concentrations (Figure 11), plasma jets again provide the highest median concentrations, followed by DBDs and corona discharges. The reported median of NO_2^- concentrations produced using Plasma jet and DBD are higher when treating tap water than pure one. In contrast, corona discharge exhibits almost the same median value, indecently from the used water. The data related to NO_3^- concentrations (Figure 11) confirm the previously observed trend, wherein the plasma jets have the highest median NO_3^- concentrations. In this instance, the corona discharge and plasma jet sources produce higher median concentrations when treating tap water than pure water. Notably, nitrate concentrations in tap water can be affected by the presence of nitrates in the untreated water itself

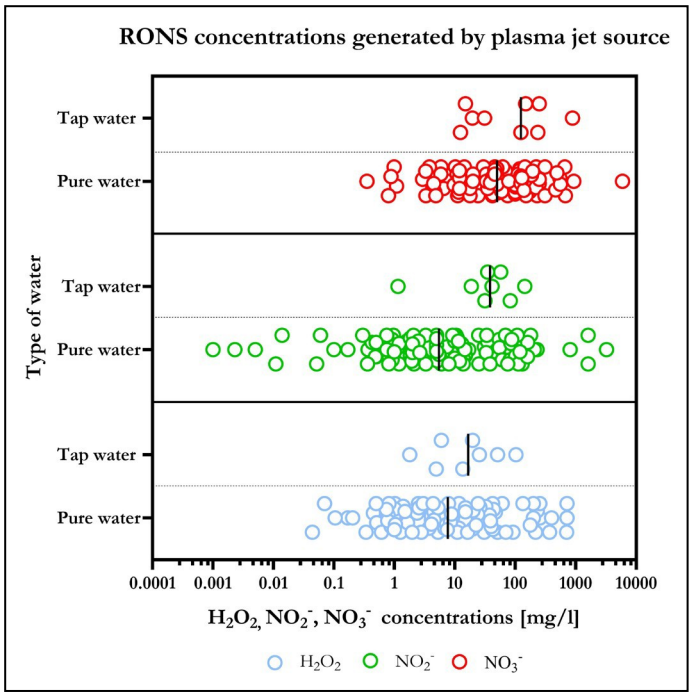

Figure 8: Influence of the type of water on concentrations of RONS (H_2O_2, NO_2^-, NO_3^-), produced with plasma jet CAP source. The black line represents the median.

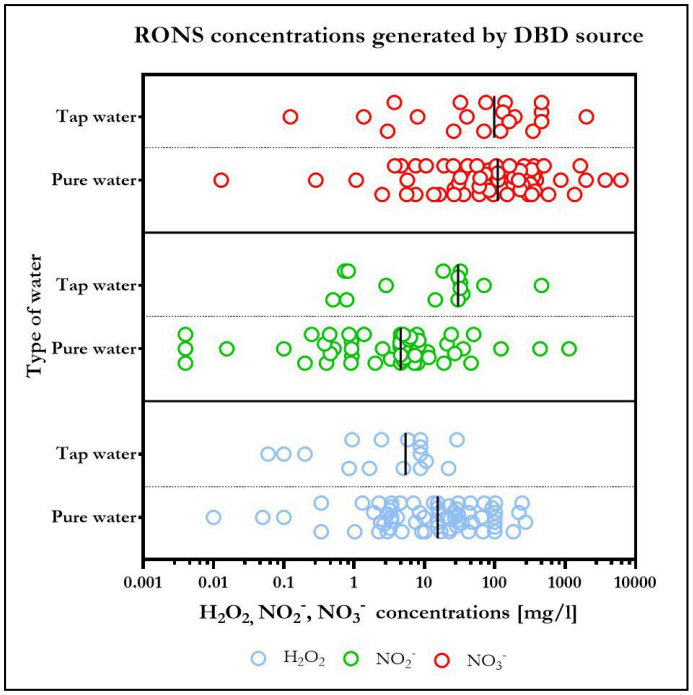

Figure 9: Influence of the type of water on concentrations of RONS (H_2O_2, NO_2^-, NO_3^-), produced with DBD CAP source. The black line represents the median.

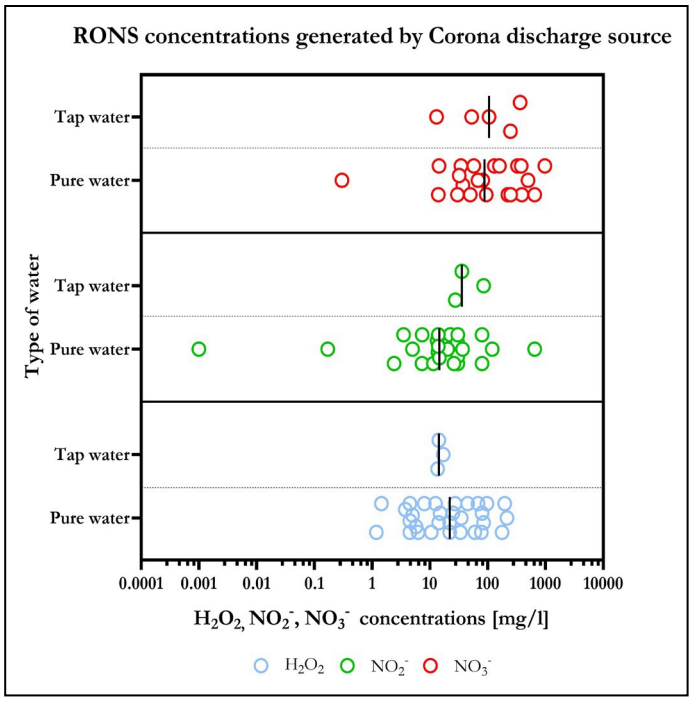

Figure 10: Influence of the type of water on concentrations of RONS (H_2O_2, NO_2^-, NO_3^-), produced by corona discharge CAP source. The black line represents the median.

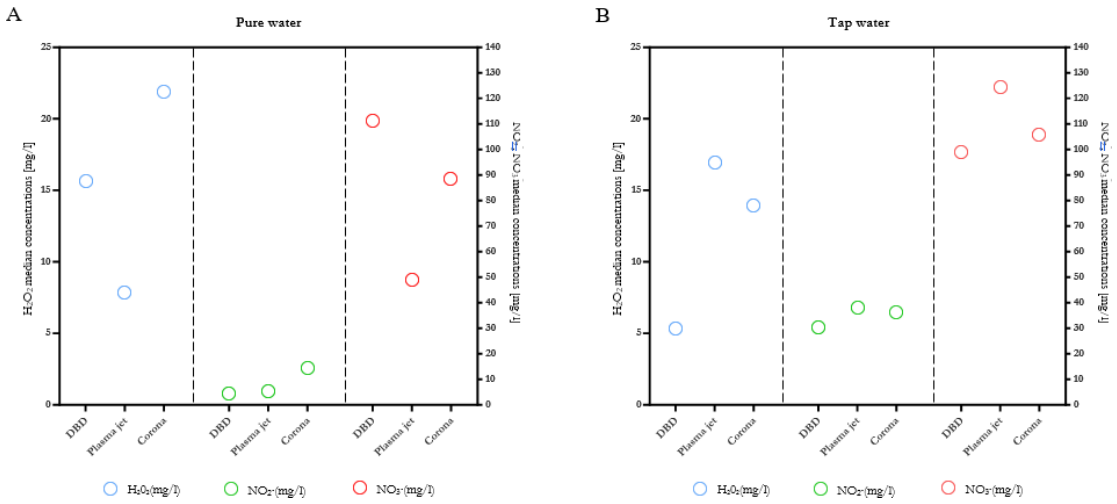

Figure 11: Median value of concentrations of RONS (H_2O_2, NO_2^-, NO_3^-), produced by DBD, Plasma jet and Corona discharge in pure (a) or tap (b) water.

2.3.4 Influence of type of water, volume, and plasma sources on RONS concentration.

Figures 12-16 illustrate the correlation between the volume (in liters) and concentrations (mg/l) of H_2O_2, NO_2^-, and NO_3^- in pure and tap water treated using CAP sources. Figure 12a depicts the H_2O_2 concentration distribution in pure water. Few papers report a treated volume higher than 0.5 l; only those under 0.25 l reach the highest concentrations (200 mg/l). Conversely, in tap water (Figure 12b), H_2O_2 concentrations are markedly lower, with maximum values of 28 mg/l.

Figure 13a displays NO_2^- concentrations; almost all the papers report treated volumes lower than 0.5 l, and exclusively, treated volumes below 0.4 l report the highest concentrations (230 mg/l). In this instance, the plasma jet and gliding arc yield the highest concentrations. NO_2^- concentrations in tap water (Figure 13b) are lower than in pure water, with many papers reporting concentrations below 50 mg/l.

NO_3^- concentrations in pure water (Figure 14a) reveal a wide distribution across different CAP sources. As reported for NO_2^- and H_2O_2, also in this case, the major part of the paper reports treated volumes below 0.5 l, and those under 0.25 l are the highest concentrations (500 mg/l) of nitrate, achieved with plasma jet and gliding arc. Figure 14b depicts NO_3^- concentrations in tap water, showing similar maximum values to those in pure water. These graphs demonstrate the differential impact of various cold plasma sources on generating RONS in pure versus tap water, highlighting the influence of the treated volume on the concentration of different RONS.

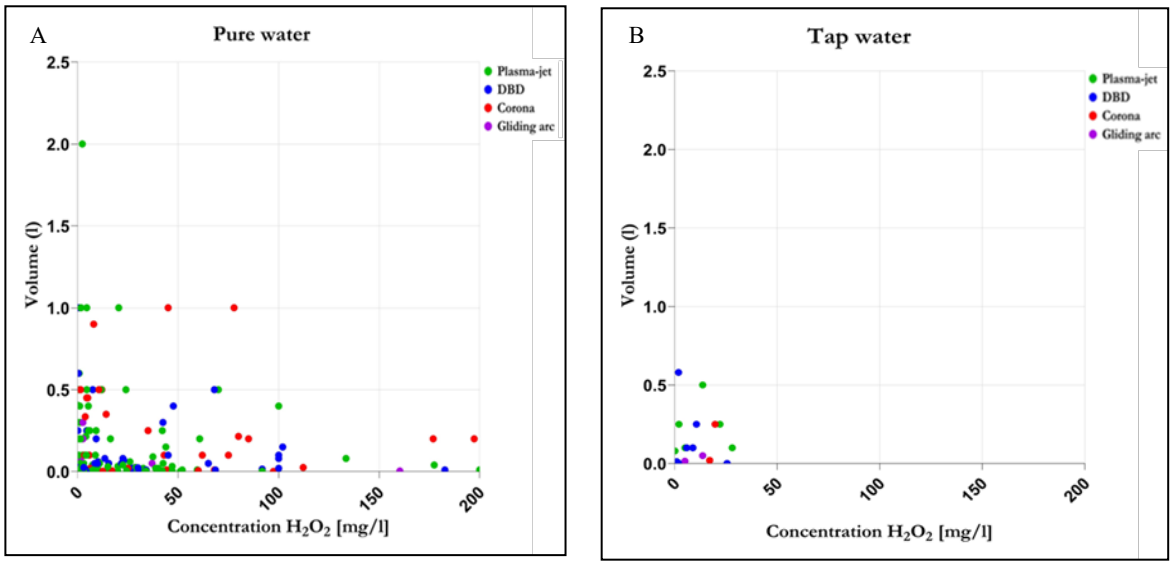

Figure 12: Influence of treated volume and CAP source on H_2O_2 concentration in pure (a) and tap (b) water.

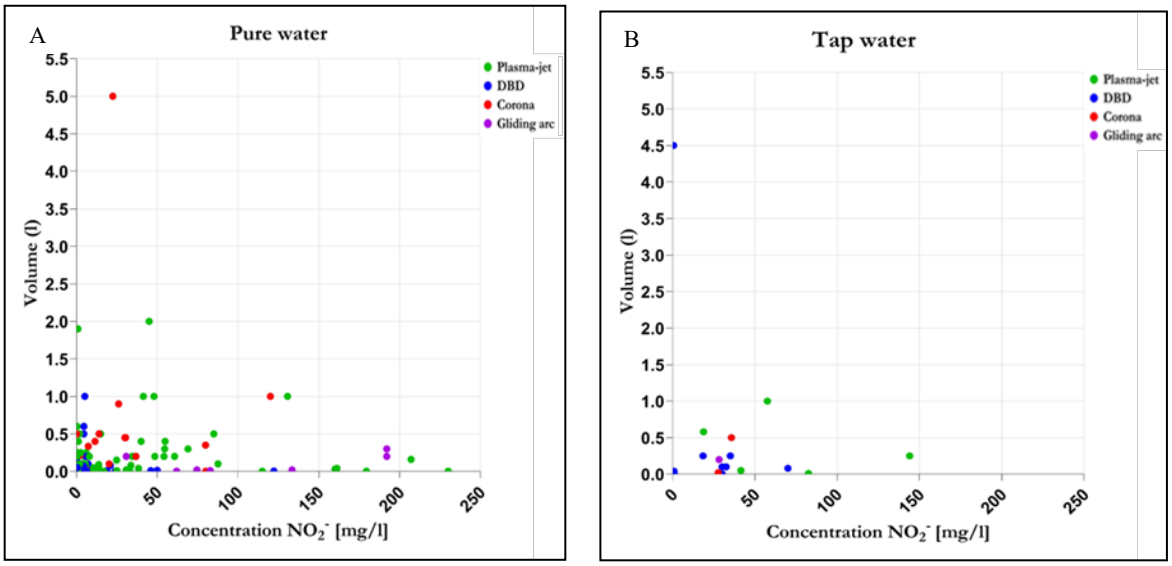

Figure 13: Influence of treated volume and CAP source on NO_2^- concentration in pure(a) and tap (b) water.

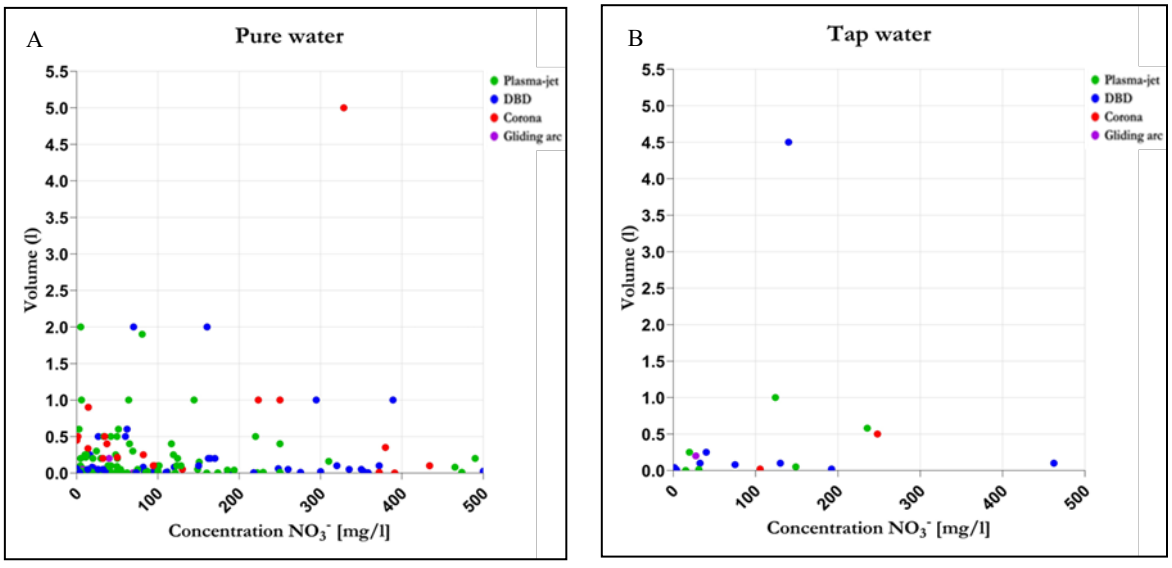

Figure 14: Influence of treated volume and CAP source on NO_3^- concentration in pure (a) and tap (b) water.

2.3.5 Influence of the type of water, gas, and plasma sources on pH value.

Figure 15 reports the pH values of pure and tap water treated with multiple working gases and subjected to plasma jet, DBD, and corona discharge CAP sources (excluding gliding arc due to a lack of data, only 15 papers). Plasma jet treatments in pure water (Figure 15 a) lead to lower median pH levels than tap water, regardless of the processed gas. Air leads to the highest acidification potential (median pH = 3), succeeded by Argon (median pH= 3.9), Helium (median pH=4.2), and nitrogen (median pH=5). The median pH related to plasma jet tap water treatments is higher than that of pure water, which is nearer to neutral levels. Indeed, all median pH values fall within 6 and 7.5 when treating tap water due to weak carbonate buffering capacity in tap water. Figure 15 b hinders a comprehensive assessment of the pH induced by DBD treatment of water. DBD generated in air (Figure 17b) induces higher pure and tap water acidification than air plasma jet treatments. Figure 15 c shows pH values observed after pure and tap water corona discharge treatments. For pure water, air leads to the highest level of acidification, with a median pH of 3, indicating a strong acidic environment. Argon-treated water follows, with a median pH of 3.9, suggesting a slightly less acidic outcome. Helium and nitrogen PAW treatment report median pH of 4.2 and 5, which is still acidic but less than the other gases mentioned. In contrast, treatments performed on tap water result in pH values that are closer to neutral values.

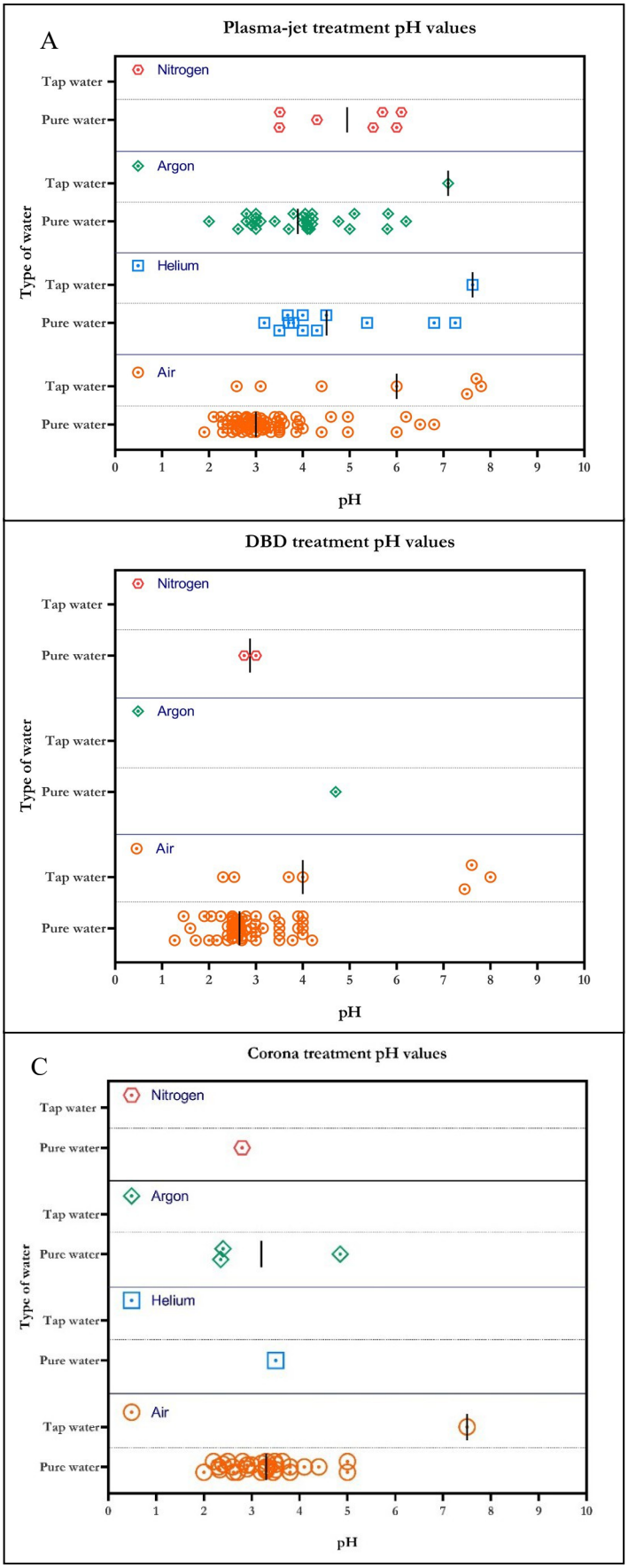

Figure 15: Influence of type of water and working gas on pH value using Plasma jet (a), DBD (b), and Corona (c) source. The black line represents the median.

2.3.6 Correlation between quantity and concentrations of RONS depending on CAP source and type of water.

Figures 16-18 show a comparative analysis of the quantities (mg) and concentrations (mg/l) of H_2O_2, NO_2^-, and NO_3^- measured after various plasma-water treatment methods. Each chart features two dashed lines representing the mean values of the reported parameters, dividing the plots into four quadrants.

Figure 16a presents the quantities of H_2O_2 in pure water. Data points from all CAP sources fall within the quadrant characterized by below-average values in both quantity and concentration. The highest H_2O_2 concentrations are equally found in the upper and bottom right quadrant, highlighting highest quantities related to the highest reported concentrations. Notably, corona discharge and plasma jet treatments reveal the highest H_2O_2 quantities.

Figure 17a presents the quantities and concentrations of NO_2^-. Data points cluster in the quadrant denoted by below-average values for quantity and concentration. The highest nitrite concentrations occur below the average quantities, although many cases are reported where above-average concentrations correspond to above-average quantities. Plasma jet treatments produce the highest NO_2^- quantities, while DBD treatments provide the lowest concentrations compared to the other CAP sources.

The analysis of NO_3^- quantities in pure water (Figure 18a) shows that the data set is mainly grouped below the average quantities, regardless of the CAP source. The highest NO_3^- concentrations are seldom observed above the mean quantity values. Plasma jet provides the highest NO_3^- quantities. Contrary to NO_2^- observations, the DBD is significantly represented in the fourth quadrant, emphasizing the production of above NO_3^- mean concentrations.

Figures 16b, 17b and 18b depict the RONS quantities treating tap water. H_2O_2 quantities in tap water (Figure 16b) reveal a marked reduction in the mean production across all CAP sources compared to pure

water treatment. The plasma jet shows a slight advantage in producing H_2O_2, although its mean production is reduced compared to pure water. The NO_2^- mean quantity in tap water (Figure 17b) is higher (9 mg) than in pure water treatment (5 mg). The plasma jet induces relatively higher NO_2^- concentrations than other sources, although its efficacy is lower than in pure water. Figure 18b illustrates the quantities and concentrations of NO_3^- in tap water. Despite the reduction in mean concentrations compared to pure water, the average quantity remains similar to that in pure water. Plasma jet and corona discharge produce the highest quantities of RONS.

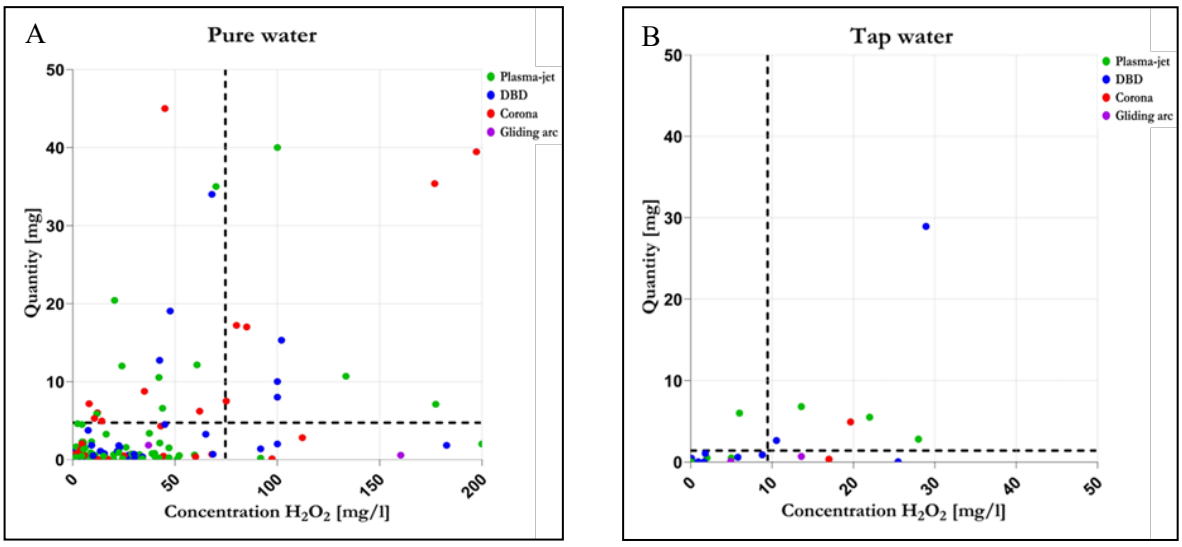

Figure 16: Correlation between quantity and concentration of H_2O_2 in pure (a) and tap (b) water (right) depending on the type of CAP source. Dashed lines represent the mean values.

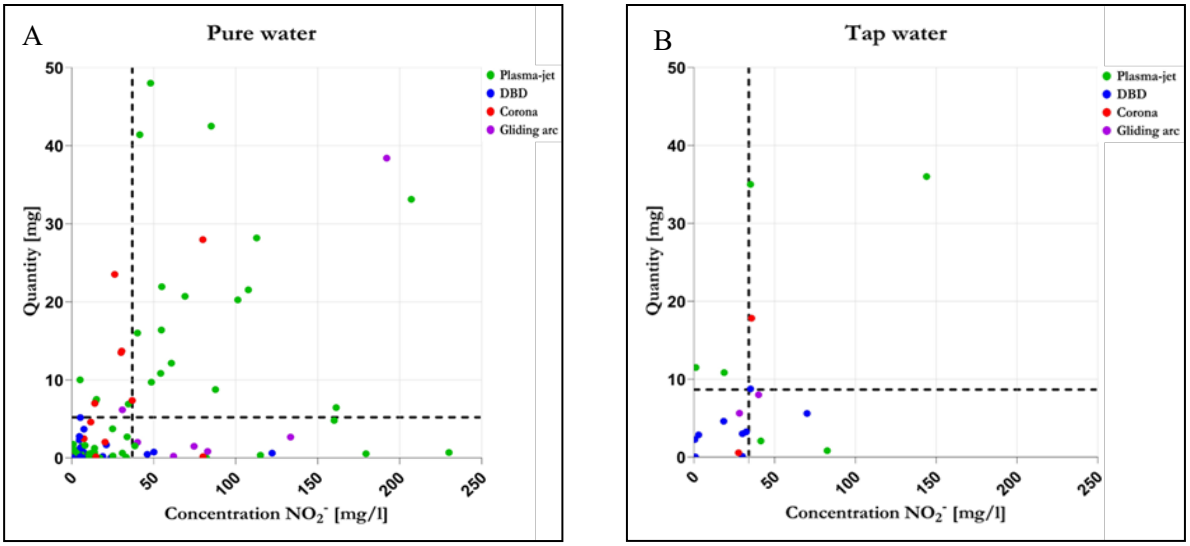

Figure 17: Correlation between quantity and concentration of NO_2^- in pure (a) and tap (b) water, depending on the type of CAP source. Dashed lines represent the mean values.

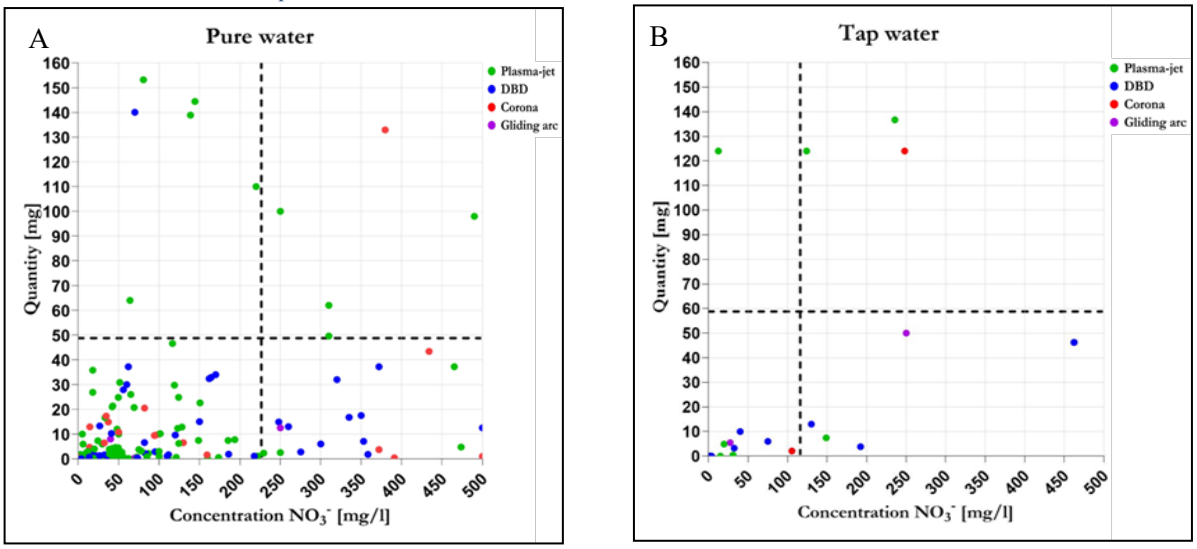

Figure 18: Correlation between quantity and concentration of NO_3^- in pure (a) and tap (b)water, depending on the type of CAP source. Dashed lines represent the mean values.

2.3.7 Correlation between the mean energy density and concentration of RONS depending on the type of plasma source.

Figures 19, 20, and 21 present a detailed analysis of the mean energy density (kWh/l) delivered in the PAW production process using multiple CAP sources: plasma jet, DBD, corona, and gliding arc. Each scatter plot displays the concentration of H_2O_2, NO_2^- and NO_3^- versus the mean energy density, with performance boundaries for each source highlighted by dashed boxes.

Figure 19 displays the concentration of hydrogen peroxide against mean energy density. The DBD and plasma jet exhibit the broadest range of mean energy densities, but only the DBD reaches the highest concentrations. The corona discharge operates within a more limited density range and results in lower concentrations than DBD. The plasma jet and gliding arc require among the highest energy densities, even if the H_2O_2 concentrations are limited.

Figure 20 reports the concentration of nitrites versus the mean energy density. The DBD produces significant NO_2^- concentrations using a broad range of high energy density values. While capable of reaching high concentrations, the gliding arc and plasma jet reveal lower energy densities than the DBD. The plasma jet shows moderate mean energy values and is constrained within lower concentrations than DBD and gliding arc.

Figure 21 illustrates the concentrations of nitrates and mean energy density. The plasma jet and DBD provided the highest NO_3^- concentrations, but only DBD is associated with the highest mean energy density value. The plasma jets operate within a lower energy density range than the DBD but exhibit similar maximum concentrations. Corona discharge and gliding arc show lower concentrations than DBD and plasma jet, with lower mean energy density than DBD. These graphs highlight the varying efficiencies of plasma treatment methods in producing RONS in pure water. The DBD is the most versatile and capable of operating across a wide range of mean energy densities and can produce the highest concentration of hydrogen peroxides, nitrites, and nitrates. Although each treatment exhibits

distinct average energy densities and RONS concentrations, they all share treated volumes characteristic of laboratory scales (below 0.5 l). The highest mean energy densities in each graph are related to Park *et al* [57]. This article shows a PAW treatment based on a DBD source, treating 3 ml of distilled water for 10 min. The recorded discharge power is 61 W, and the final pH of the treated liquid is 3.5. The reported concentrations of H_2O_2, NO_2^- and NO_3^- are 34 mg/l, 240 mg/l and 60 mg/l. Although this paper presents the highest mean energy density among those analyzed, it only corresponds to the highest concentrations in the case of nitrites. Rathore *et al* [58] report the highest concentrations of hydrogen peroxides, with a DBD source employed to treat 20 ml of distilled water for 15 minutes at a discharge power of 30 W, inducing a hydrogen peroxide concentration of 103 mg/l. Finally, Miranda *et al* [59] report the highest concentrations of nitrates. In this study, the PAW process utilized a DBD source to treat 25 ml of distilled water for 10 minutes, with a final nitrate concentration equal to 500 mg/l.

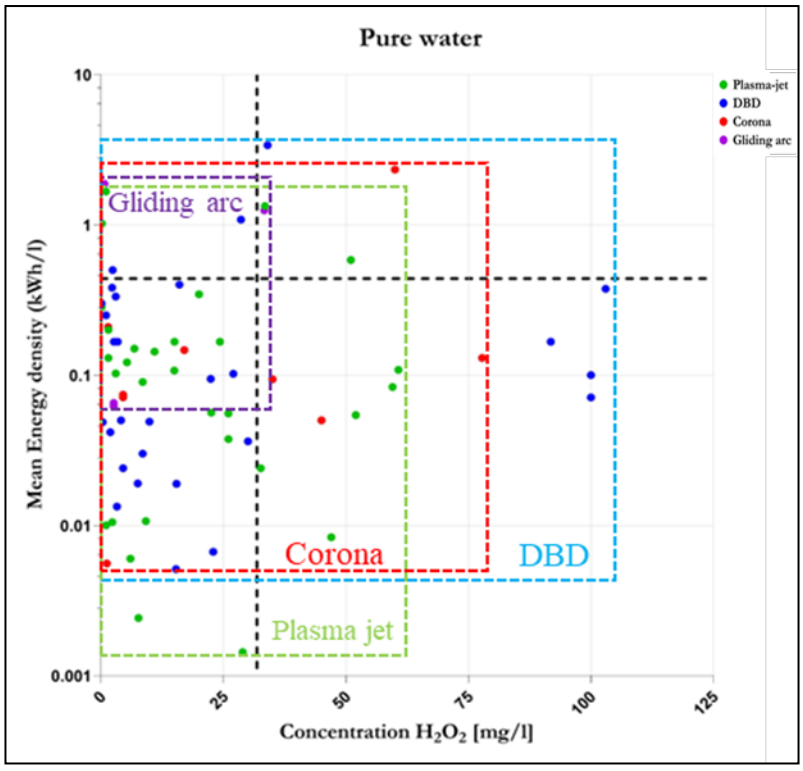

Figure 19: Correlation between mean energy density and concentration of H_2O_2 in pure water, depending on the type of plasma source. Black dashed lines represent the mean values.

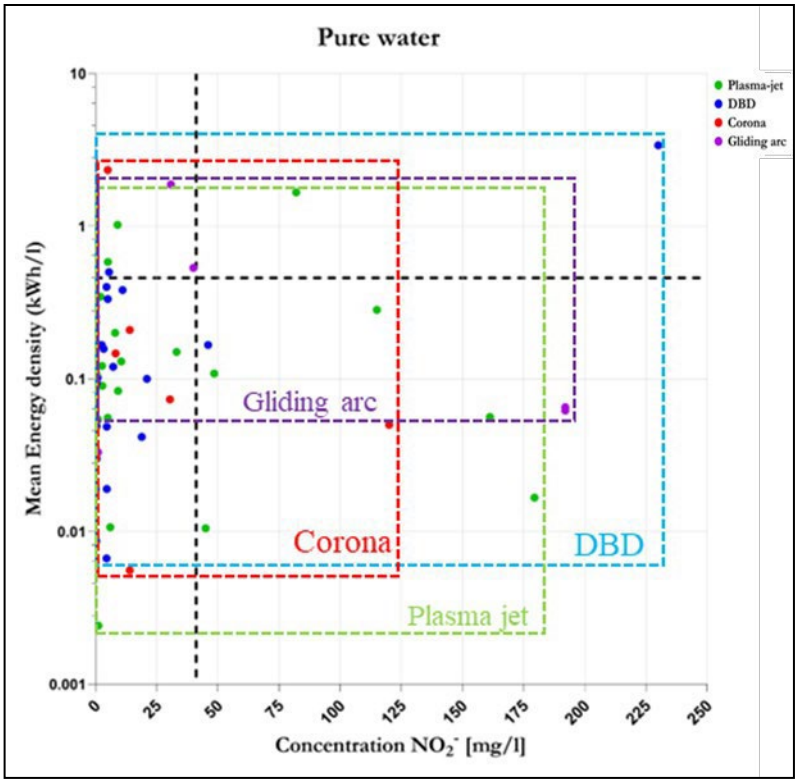

Figure 20: Correlation between mean energy density and concentration of NO_2^- in pure water, depending on the type of plasma source. Black dashed lines represent the mean values.

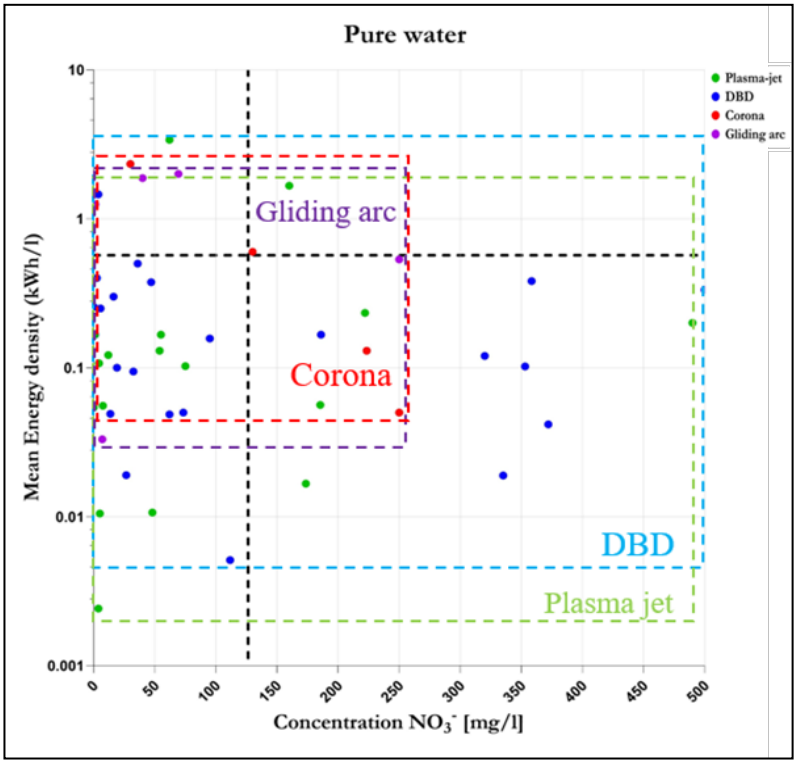

Figure 21: Correlation between mean energy density and concentration of NO_3^- in pure water, depending on the type of plasma source. Dashed lines represent the mean values.

2.3.8 Influence of type of water and plasma source on the efficiency of RONS production.

Since the energy spent to generate plasma is used to produce various species, among which the long-lived ones are hydrogen peroxide, nitrites, and nitrates, an important parameter to compare the processes, especially for potential industrial scale-up, is the efficiency of RONS production. This parameter has been calculated by dividing the molar amounts of hydrogen peroxide, nitrites, and nitrates by energy consumption. Figure 22 illustrates the efficiency of RONS production in pure and tap water. Figure 22a reports the efficiency of RONS production in pure water, covering a broader range of efficiency values than tap water. The highest efficiencies result close to 1mol/kWh and are related to the studies of Xu Z. [60] using a plasma jet for the treatment of 3 ml of pure water, and Bălan G. [61], where 300 ml of distilled water are exposed to a gliding arc for 10 min. However, many studies report much lower efficiencies, clustering around 0.01 to 0.1 mol/kWh. Figure 22b focuses on RONS production efficiency in tap water; the efficiency values vary significantly among the studies, spanning from approximately 0.001 to 1 mol/kWh. Notably, the study by Xiao A. (2022) [62] reports a DBD treatment of 1 l of tap water for 1 h, resulting in the highest efficiency among the analised paper dealing with plasma treatments of TAP water, about 1 mol/kWh. Fig. 22 and 23 reveals that the efficiency of RONS production in pure water tends to be higher than in tap water. The top-performing studies in both water types achieve similar maximum efficiencies, indicating that high RONS production efficiency is achievable in both water media with optimized conditions.

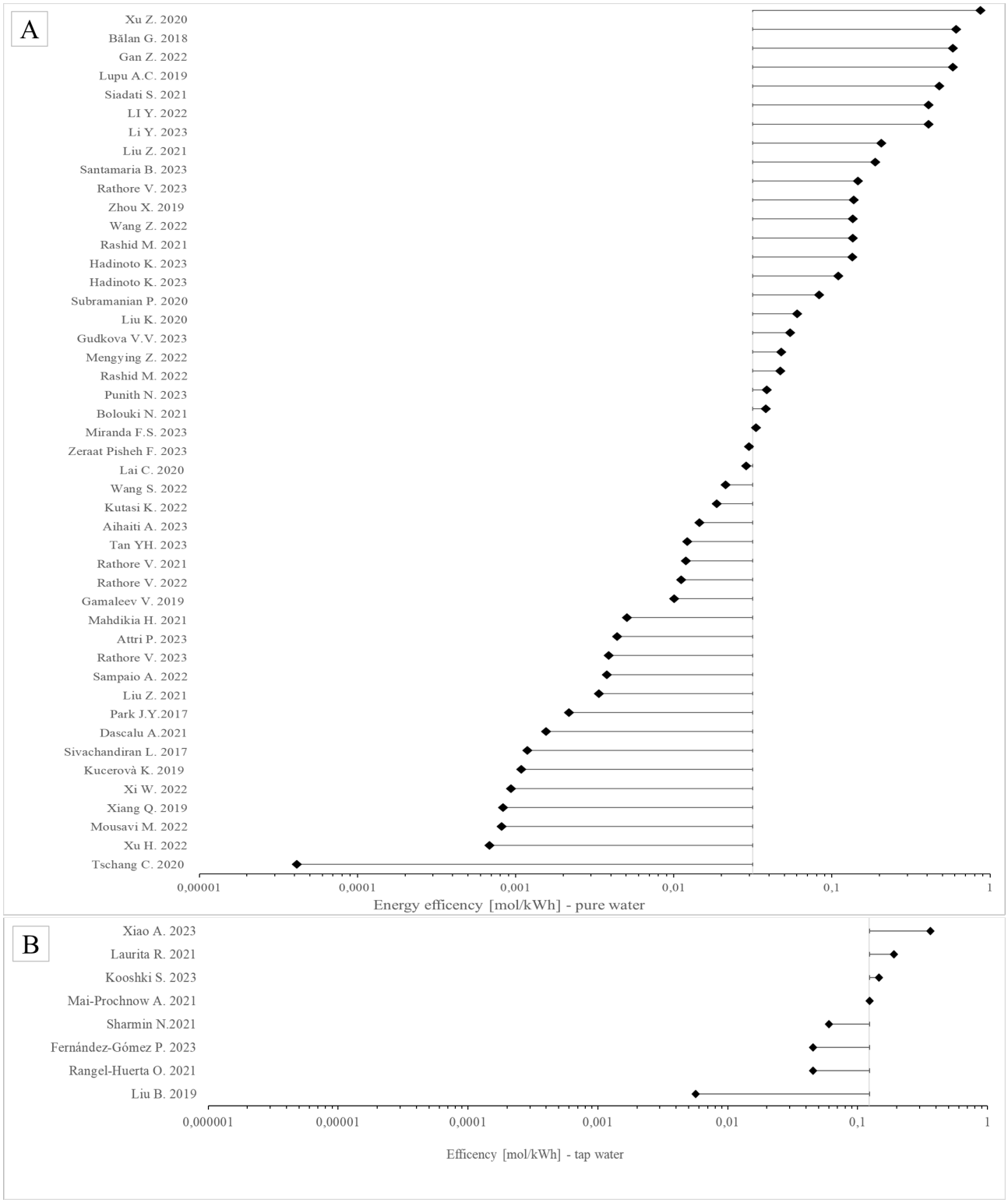

Figure 22: Efficiency of RONS production in pure (a) and tap (b) water. The vertical line represents the median.

2.4 Conclusion

This systematic review highlights the various methodologies evidenced within the PAW production reported in 358 original studies from 2017 to 2023. The presented study systematically correlates the plasma-water process parameters with the pH levels and RONS concentrations in PAW and reports results concerning the average energy density and the efficiency of RONS production.

Examining multiple CAP sources, particularly the plasma jets, DBDs, and corona discharges, underlines their distinct influences on RONS production. Figures 19-24 demonstrate that the plasma jet produces the highest average quantities of RONS in pure and tap water, although the treated volumes are predominantly on a laboratory scale. Our findings suggest that despite specific methods permitting high RONS concentrations, the overall efficiency of RONS production is generally low, with most values reported by the studies below 0.1 mol/kWh, as demonstrated in Figures 28 and 29. A critical remark concerns the energy densities. It is worth noting that the heat capacity of water is 4182 J/kg·K; thus, processes in which the average energy density exceeds 334.6 J/ml, i.e. 0.093 kWh/l, if entirely transferred to the water, can cause an increase of approximately 80 K in the water temperature, leading to its boiling. This must be considered in the analysis of industrial development of PAW production processes. In addition, it should be considered that efficiency does not reflect the actual plant costs, as auxiliary systems for control or cooling of the sources may be necessary when working with large-scale plants. Particularly in the context of scaling up processes, a comprehensive assessment of both capital (mainly related to high power supplies) and operational costs will need to be considered in order to make plasma-assisted liquid production feasible for industrial processes.

Despite significant challenges in improving the efficiency of PAW production, which is essential for its practical applications, the potential of PAW remains considerable. Specific treatments have demonstrated high RONS production rates, indicating that more efficient PAW production methods can be developed with targeted research and optimization. This review advances our understanding of PAW

processes and mechanisms and sets the groundwork for future research to improve RONS production efficiency. By identifying key factors that influence the efficacy of PAW, our work provides a valuable framework for comparing future PAW production systems with the literature-reported ones.

2.5 Acknowledgments

The Authors thank the COST Action PlAgri, CA19110, supported by COST (European Cooperation in Science and Technology).

Funded by the EU NextGenerationEU through the Recovery and Resilience Plan for Slovakia under the project No. 09I03-03-V03-00033 EnvAdwice.

Funded by the EU NextGenerationEU through the Recovery and Resilience Plan for Italy under the project "PAAFOOD Plasma activated aerosol for the preservation and decontamination of fresh and minimally processed plant foods", No. 2022W43KHF_002 – CUP J53D23010480001.

References

1. C. Bradu, K. Kutasi, M. Magureanu, N. Puač, and S. Živković, "Reactive Nitrogen Species in Plasma-Activated Water: Generation, Chemistry and Application in Agriculture," *Journal of Physics D: Applied Physics* 53 (2020): 223001.

2. X. Lu, G. V. Naidis, M. Laroussi, S. Reuter, D. B. Graves, and K. Ostrikov, "Reactive Species in Non-Equilibrium Atmospheric- Pressure Plasmas: Generation, Transport, and Biological Effects," 630 (2016): 1–84.

3. S. Mohades, A. M. Lietz, and M. J. Kushner, "Generation of Reactive Species in Water Film Dielectric Barrier Discharges Sustained in Argon, Helium, Air, Oxygen and Nitrogen," *Journal of Physics D: Applied Physics* 53 (2020): 435206.

4. F. Girard, V. Badets, S. Blanc, et al., "Formation of Reactive Nitrogen Species Including Peroxynitrite in Physiological Buffer Exposed to Cold Atmospheric Plasma," *RSC Advances* 6 (2016): 78457–78467.

5. G. Uchida, A. Nakajima, T. Ito, et al., "Effects of Nonthermal Plasma Jet Irradiation on the Selective Production of H_2O_2 and NO_2^- in Liquid Water," *Journal of Applied Physics* 120 (2016): 20.

6. O. Kostya, R. Zhou, R. Zhou, et al., "Plasma-Activated Water: Generation, Origin of Reactive Species and Biological Applications," *Journal of Physics D: Applied Physics* 53 (2020): 303001.

7. J. L. Brisset and J. Pawlat, "Chemical Effects of Air Plasma Species on Aqueous Solutes in Direct and Delayed Exposure Modes: Discharge, Post-Discharge and Plasma Activated Water," *Plasma Chemistry and Plasma Processing* 36 (2016): 355–381.

8. X. Zhang, R. Zhou, K. Bazaka, et al., "Quantification of Plasma Produced OH Radical Density for Water Sterilization," *Plasma Processes and Polymers* 15 (2018): 6.

9. W. F. L. M. Hoeben, P. P. van Ooij, D. C. Schram, T. Huiskamp, A. J. M. Pemen, and P. Lukeš, "On the Possibilities of Straightforward Characterization of Plasma Activated Water," *Plasma Chemistry and Plasma Processing* 39 (2019): 597–626.

10. P. Heirman, W. Van Boxem, and A. Bogaerts, "Reactivity and Stability of Plasma-Generated Oxygen and Nitrogen Species in Buffered Water Solution: A Computational Study," *Physical Chemistry Chemical Physics* 21 (2019): 12881–12894.

11. J. Shen, H. Zhang, Z. Xu, et al., "Preferential Production of Reactive Species and Bactericidal Efficacy of Gas-Liquid Plasma Discharge'', *Chemical Engineering Journal* 362 (2019): 402-412.

12. K. Takahashi, K. Satoh, H. Itoh, et al., "Production Characteristics of Reactive Oxygen/Nitrogen Species in Water Using Atmospheric Pressure Discharge Plasmas," *Japanese Journal of Applied Physics* 55 (2016): 7S2.

13. Z. Machala, B. Tarabová, D. Sersenová, M. Janda, and K. Hensel, "Chemical and Antibacterial Effects of Plasma Activated Water: Correlation With Gaseous and Aqueous Reactive Oxygen and Nitrogen Species, Plasma Sources and Air Flow Conditions," Journal of Physics D: Applied Physics 52 (2019): 034002.

14. C. Y. Hou, Y. C. Lai, C. P. Hsiao, et al., "Antibacterial Activity and the Physicochemical Characteristics of Plasma Activated Water on Tomato Surfaces," *LWT* 149 (2021): 111879.

15. S. Mitra, M. Veerana, E. H. Choi, and G. Park, "Effects of Pre-Treatment Using Plasma on the Antibacterial Activity of Mushroom Surfaces," *Foods* 10 (2021): 1888.

16. Q. Xiang, C. Kang, L. Niu, D. Zhao, K. Li, and Y. Bai, "Antibacterial Activity and a Membrane Damage Mechanism of Plasma-Activated Water Against *Pseudomonas deceptionensis* CM2," *LWT* 96 (2018): 395−401.

17. M. Ali, J. H. Cheng, and D. W. Sun, "Combined Application of Ascorbic and Oxalic Acids Delays Postharvest Browning of Litchi Fruits Under Controlled Atmosphere Conditions," *Food Chemistry* 350 (2021): 129277.

18. D. Yan, J. H. Sherman, and M. Keidar, "Cold Atmospheric Plasma, a Novel Promising Anti-Cancer Treatment Modality," *Oncotarget* 8 (2017): 15977−15995.

19. B. Pang, Z. Liu, S. Wang, et al., "Discharge Mode Transition in a He/Ar Atmospheric Pressure Plasma Jet and Its Inactivation Effect Against Tumor Cells In Vitro," *Journal of Applied Physics* 130 (2021): 15.

20. L. Gan, J. Jiang, J. W. Duan, et al., "Cold Atmospheric Plasma Applications in Dermatology: A Systematic Review," *Journal of Biophotonics* 14 (2021): e202000415.

21. Z. Liu, Y. Zheng, J. Dang, et al., "A Novel Antifungal Plasma- Activated Hydrogel," *ACS Applied Materials & Interfaces* 11 (2019): 22941−22949.

22. Y. Li, M. H. Kang, H. S. Uhm, G. J. Lee, E. H. Choi, and I. Han, "Effects of Atmospheric-Pressure Non-Thermal Bio-Compatible Plasma and Plasma Activated Nitric Oxide Water on Cervical Cancer Cells," *Scientific Reports* 31 (2017): 7.

23. A. Vaid, C. Patil, A. Sanghariyat, et al., "Emerging Advanced Technologies Developed by IPR for Bio MedicalApplications—A Review," *Neurology India* 68 (2020): 26–34.

24. D. Boehm, J. Curtin, P. J. Cullen, and P. Bourke, "Hydrogen Peroxide and Beyond-the Potential of High-Voltage Plasma-Activated Li- quids Against Cancerous Cells," *Anti-Cancer Agents in Medicinal Chemistry* 18 (2018): 815–823.

25. S. Raud, J. Raud, I. Jõgi, et al., "The Production of Plasma Activated Water in Controlled Ambient Gases and Its Impact on Cancer Cell Viability," *Plasma Chemistry and Plasma Processing* 41 (2021): 1381–1395.

26. A. Bisag, P. Isabelli, R. Laurita, et al., "Cold Atmospheric Plasma Inactivation of Aerosolized Microdroplets Containing Bacteria and Purified SARS-CoV-2 RNA to Contrast Airborne Indoor Transmission," *Plasma Processes and Polymers* 17 (2020): 2000154.

27. A. Bisag, P. Isabelli, G. Laghi, et al., "Cold Atmospheric Plasma Decontamination of SARS-CoV-2 Bioaerosols," *Plasma Processes and Polymers* 19 (2022): e2100133.

28. N. Puač, M. Gherardi, and M. Shiratani, "Plasma Agriculture: A Rapidly Emerging Field," *Plasma Processes and Polymers* 15 (2018): 2.

29. F. Judée, S. Simon, C. Bailly, and T. Dufour, "Plasma-Activation of Tap Water Using DBD for Agronomy Applications: Identification and Quantification of Long Lifetime Chemical Species and Production/ Consumption Mechanisms," *Water Research* 133 (2018): 47–59.

30. K. Kučerová, M. Henselová, Ľ. Slováková, and K. Hensel, "Effects of Plasma Activated Water on Wheat: Germination, Growth Parameters, Photosynthetic Pigments, Soluble Protein Content, and Antioxidant Enzymes Activity," *Plasma Processes and Polymers* 16 (2019): 1800131.

31. M. Bafoil, A. Jemmat, Y. Martinez, et al., "Effects of Low Temperature Plasmas and Plasma Activated Waters on *Arabidopsis thaliana* Germination and Growth," *PLoS One* 13 (2018): e0195512.

32. L. Sivachandiran and A. Khacef, "Enhanced Seed Germination and Plant Growth by Atmospheric Pressure Cold Air Plasma: Combined Effect of Seed and Water Treatment," *RSC Advances* 7 (2017): 1822–1832.

33. Y. Tanakaran, V. Luang-In, and K. Matra, "Effect of Atmospheric Pressure Multicorona Air Plasma and Plasma-Activated Wateron Germination and Growth of Rat-Tailed Radish Seeds," *IEEE Transactions on Plasma Science* 49 (2021): 563−572.

34. C. Alves, F. De Menezes, J. De, and O. Vitoriano, "Effect of Plasma-Activated Water on Soaking, Germination, and Vigor of Erythrina Ve- lutina Seeds," *Plasma Medicine* 9 (2019): 111−120.

35. S. Z. Ismail, M. M. Khandaker, N. Mat, and A. N. Boyce, "Effects of Hydrogen Peroxide on Growth, Development and Quality of Fruits: A Review," *Journal of Agronomy* 14 (2015): 331−336.

36. P. Dimitrakellis, M. Giannoglou, Z. M. Xanthou, E. Gogolides, P. Taoukis, and G. Katsaros, "Application of Plasma-Activated Water as an Antimicrobial Washing Agent of Fresh Leafy Produce," *Plasma Processes and Polymers* 18 (2021): 2100030.

37. R. Dhivya, V. C. Rajakrishnapriya, K. Sruthi, D. V. Chidanand, C. K. Sunil, and A. Rawson, "Biofilm Combating in the Food Industry: Overview, Non-Thermal Approaches, and Mechanisms," *Journal of Food Processing and Preservation* 46 (2022): 10.

38. C. Sarangapani, L. Scally, M. Gulan, and P. J. Cullen, "Dissipation of Pesticide Residues on Grapes and Strawberries Using Plasma-Activated Water," *Food and Bioprocess Technology* 13 (2020): 1728−1741.

39. J. Qian, H. Zhuang, M. M. Nasiru, U. Muhammad, and J. Zhang, "W. Yan. "Action of Plasma-Activated Lactic Acid on the Inactivation of Inoculated Salmonella Enteritidis and Quality of Beef," *Innovative Food Science and Emerging Technologies* 1 (2019): 57.

40. R. Zhou, R. Zhou, A. Mai-Prochnow, et al., "Surface Plasma Dis- charges for the Preservation of Fresh-Cut Apples: Microbial Inactivation and Quality Attributes," *Journal Physics D: Applied Physics* 53 (2020): 17.

41. R. Laurita, G. Gozzi, S. Tappi, et al., "Effect of Plasma Activated Water (PAW) on Rocket Leaves Decontamination and Nutritional Value," *Innovative Food Science and Emerging Technologies* 73 (2021): 102805.

42. J. Barrales Astorga, K. Hadinoto, P. Cullen, S. Prescott, and F. J. Trujillo, "Effect of Plasma Activated Water on the Nutritional Composition, Storage Quality and Microbial Safety of Beef," *LWT* 154 (2022): 112794.

43. F. Capelli, S. Tappi, T. Gritti, et al. "Decontamination of Food Packages From SARS-COV-2 RNA With a Cold Plasma-Assisted System," *Applied Sciences* 1 (2021): 9.

44. M. R. Webb and G. M. Hieftje, "Spectrochemical Analysis by Using Discharge Devices With Solution Electrodes," *Analytical Chemistry* 81 (2009): 862−867.

45.M. Smoluch, P. Mielczarek, and J. Silberring, "Plasma-Based Ambient Ionization Mass Spectrometry in Bioanalytical Sciences," *Mass Spectrometry Reviews* 35 (2016): 22−34.

46. A. T. Ambujakshan, J. M. Pringle, Z. Chen, et al., "An Environmentally Friendly In Situ Plasma and Anodization Method to Produce Titanium Dioxide Nanotubes," *Plasma Processes and Polymers* 1 (2018): 15.

47. G. Laghi, D. Franco, G. G. Condorelli, et al., "Control Strategies for Atmospheric Pressure Plasma Polymerization of Fluorinated Silane Thin Films With Antiadhesive Properties," *Plasma Processes and Polymers* 20 (2023):2200194.

48.U. Cvelbar, J. L. Walsh, M. Černá,ket al., "White Paper on the Future of Plasma Science and Technology in Plastics and Textiles," *Plasma Processes and Polymers* 16 (2019): 1.

49.H. Malekzad, T. Gallingani, F. Barletta, et al. "Single-Step Deposition of Hexamethyldisiloxane Surface Gradient Coatings With a High Amplitude of Water Contact Angles Over a Polyethylene Foil," *Plasma Processes and Polymers* 1 (2021):2.

50.M. J. Page, J. E. McKenzie, P. M. Bossuyt, et al., "The PRISMA 2020 Statement: An Updated Guideline for Reporting Systematic Reviews," *British Medical Journal* 372 (2021): 71.

51.B. Surowsky, O. Schlter, and D. Knorr, "Interactions of Non-Thermal Atmospheric Pressure Plasma With Solid and Liquid Food Systems: A Review," *Food Engineering Reviews* 7 (2015): 82−108.

52.K. KučerováZ. Machala, and K. Hensel, "Transient Spark Discharge Generated in Various N_2/O_2 Gas Mixtures: Reactive Species in the Gas and Water and Their Antibacterial Effects," *Plasma Chemistry and Plasma Processing* 40 (2020):749−773.

53. F. G. Chizoba Ekezie, D. W. Sun, and J. H. Cheng, "A Review on Recent Advances in Cold Plasma Technology for the Food Industry: Current Applications and Future Trends," Trends in Food Science & Technology 69 (2017): 46–58.

54. P. Starič, K. Vogel-Mikuš, M. Mozetič, and I. Junkar, "Effects of Nonthermal Plasma on Morphology, Genetics andPhysiology of Seeds: A Review," Plants 9 (2020): 1736.

55. K. Adesina, T. C. Lin, Y. W. Huang, M. Locmelis, and D. Han, “A Review of Dielectric Barrier Discharge Cold Atmospheric Plasma for Surface Sterilization and Decontamination,” IEEE Transactions on Radiation and Plasma Medical Sciences 8 (2024): 295–306.

56. J. Pawłat, P. Terebun, M. Kwiatkowski, et al., “Evaluation of Oxi- dative Species in Gaseous and Liquid Phase Generated by Mini-Gliding Arc Discharge,” Plasma Chemistry and Plasma Processing 39 (2019): 627–642.

57. J. Y. Park, S. Park, W. Choe, H. I. Yong, C. Jo, and K. Kim, “Plasma- Functionalized Solution: A Potent Antimicrobial Agent for Biomedical Applications From Antibacterial Therapeutics to Biomaterial Surface Engineering,” ACS Applied Materials & Interfaces 9 (2017):43470–43477.

58. V. Rathore, C. Patil, and A. Sanghariyat, “S. K. Nema. "Design and Development of Dielectric Barrier Discharge Setup to Form Plasma- Activated Water and Optimization of Process Parameters,” European Physical Journal D 76 (2022): 5.

59. F. S. Miranda, V. K. F. vares, M. P. Gomes, et al., “Physicochemical Characteristics and Antimicrobial Efficacy of Plasma-Activated Water Produced by an Air-Operated Coaxial Dielectric Barrier Discharge Plasma,” Water 15 (2023):23.

60. Z. Xu, X. Zhou, W. Yang, et al., Plasma Processes and Polymers 17 (2020): 8.

61. G. G. Bălan, I. Roșca, E. L. Ursu, et al., “Plasma-Activated Water: A New and Effective Alternative for Duodenoscope Reprocessing,” Infection and Drug Resistance 11 (2018): 727–733.

62. A. Xiao, D. Liu, and Y. Li, “Plasma-Activated Tap Water Production and Its Application Inatomization Disinfection,” Applied Science 13 (2023): 3015.

The article *“Production and Chemical Composition of Plasma Activated Water: A Systematic Review and Meta-Analysis”* by Montalbetti, R., Machala, Z., Gherardi, M., & Laurita, R. is published in Plasma Processes and Polymers, 2025; 22:e2400249.

3 Scale-up of CAP prototype for 2 l treatment of PAW.

Plasma-activated water has been widely studied for its potential in various applications, from disinfection to agricultural uses. The interaction between cold atmospheric plasma and water produces RONS, which endow PAW with unique biological properties such as antimicrobial effects and oxidative capabilities. However, the challenge of producing sufficient quantities of PAW for industrial applications remains significant.

As demonstrated in the systematic review of PAW production methods, the most common plasma sources, including corona discharges and Dielectric Barrier Discharges (DBDs), have been successfully used to produce PAW at the laboratory scale. While these methods generate high concentrations of RONS, their applicability in large-scale processes is often limited by the small water volumes they can treat (typically less than 0.5 liters). In industrial applications, where larger volumes of treated water are required, scaling up these plasma sources becomes necessary.

The literature consistently shows that different process parameters, such as the CAP source, treated water volume, and plasma exposure time, significantly impact the production efficiency of RONS. Specifically, larger volumes of treated water tend to result in lower RONS concentrations. Therefore, when scaling up plasma systems, it is essential to consider both the efficiency of RONS production and the volume of water that can be treated without compromising the desired chemical properties of PAW.

The current chapter addresses this need for scale-up by designing a new DBD plasma source capable of treating 2 liters of water—four times the volume previously treated by the existing corona discharge system. This chapter details the comparison between the two systems, emphasizing the technical advancements that enable the production of larger quantities of PAW while maintaining high RONS concentrations.

3.1 Corona discharge CAP source for0.5-liter treatment.

The corona discharge plasma source was the first system used for PAW production in this study and can treat 0.5 liters of distilled water (pH= 5.9). This system (Fig. 1) consists of a stainless-steel cylindrical electrode, with the tip positioned 0.5 cm above the water surface, housed inside a borosilicate glass container with a volume capacity of 0.5 liters. The corona discharge is generated by a high-voltage microsecond-pulsed generator (AlmaPulse, AlmaPlasma s.r.l.) operating at 2 kV peak voltage, a frequency of 5 kHz, and a 60% duty cycle. A magnetic stirrer is used to maintain a consistent stirring speed of 200 rpm, ensuring the homogeneity of the treated water during plasma exposure.

The corona source creates an electric field between the high-voltage electrode and the water surface, producing plasma in the air gap, directly in contact with the water surface. This plasma generates reactive species such as hydroxyl radicals (OH•), nitric oxide (NO), and superoxide (O_2^-), which dissolve into the water, producing PAW with notable antimicrobial properties.

After 10 minutes of treatment, chemical analysis of the water revealed significant concentrations of long-lived RONS (Fig. 2), including H_2O_2 13.81 ± 2.30 mg/l, NO_2^- 35.33 ± 5.40 mg/l, NO_3^- 248.45 ± 9.82 mg/l [1].

Despite the ability of the Corona discharge system to generate high RONS concentrations, its 0.5-liter capacity represents a significant limitation. This volume is insufficient for applications requiring larger quantities of PAW, such as agricultural disinfection or large-scale water treatment.

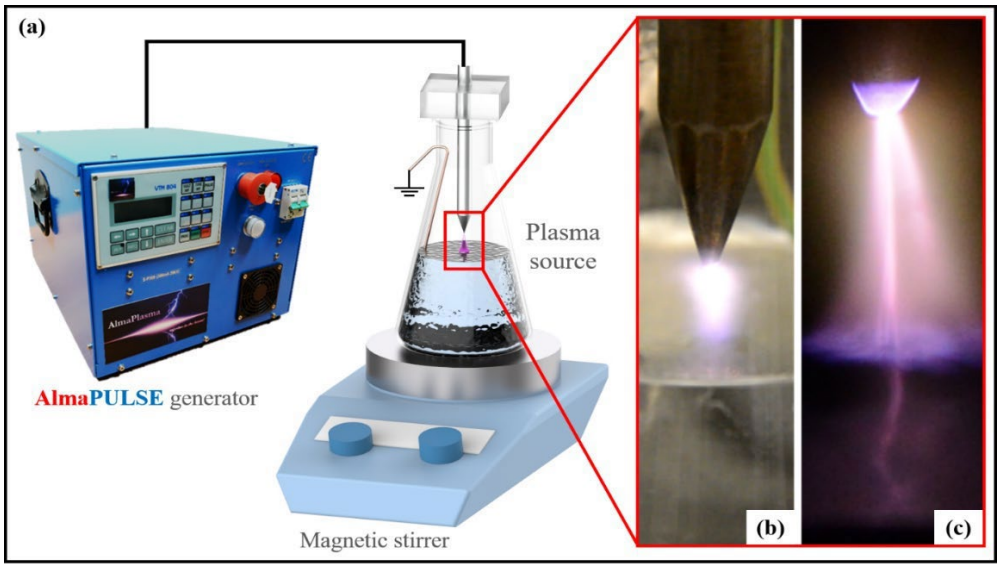

Fig 1. Corona single pin array designed for 0,5 l treatment for PAW production. All rights to this image are owned by [1].

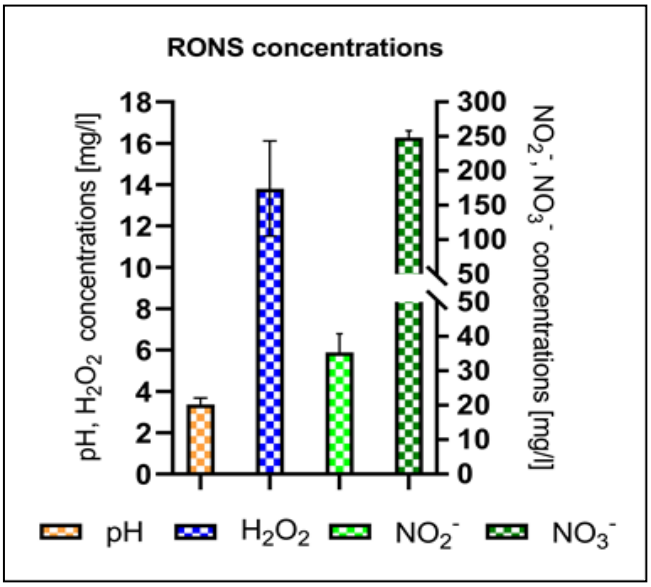

Fig. 2: pH value and RONS

3.2 Dielectric barrier discharge CAP Source for 2-liter treatment.

In response to the limitations of the Corona discharge system, a new DBD plasma source was developed to treat 2 liters of water, representing a fourfold increase in capacity compared to the Corona system. The DBD system consists of a submerged high-voltage liquid electrode and a grounded stainless-steel cylinder immersed in the water, with plasma generated in the air gap between the water surface and the DBD tip. The conductive solution in which the high-voltage electrode is immersed is created by saturating distilled water with NaCl and is contained within a glass test tube (dielectric material). The Solid Edge software was employed for the design and 3D modeling of the plasma source. This CAD (Computer-Aided Design) system allowed for the creation of a three-dimensional virtual model, which was later implemented into KeyShot (3D rendering software) to generate photorealistic images. Following this initial phase, the plasma source was partially 3D printed using a ZORTRAX M300 plus printer and partially fabricated in the Department of Industrial Engineering (DIN) mechanical workshop at Alma Mater Studiorum - University of Bologna.

This DBD system is driven by a microsecond-pulsed high-voltage generator (AlmaPULSE, Alma plasma s.r.l.) operating at a fixed frequency of 12 kHz and an average discharge power of 138.60 ± 10.6 W for distilled water. The larger volume of water treated requires more energy input than the corona discharge system.

The water is stirred at 750 rpm using a magnetic stirrer to maintain homogeneity during treatment. The treatment time is set to 22 minutes, ensuring sufficient exposure to the plasma for RONS generation. Inside the liquid electrode is a cooling system for the conductive solution. It consists of a copper helix with distilled water flowing through it, moved by a pump placed outside the plasma source. The RONS concentrations achieved with the DBD plasma source are higher than those produced by the corona discharge system in 0.5 liters of water, highlighting the success of the scale-up process (Fig. 2 and 6). The DBD system's ability to treat 2 liters of water while

maintaining high RONS concentrations makes it a more suitable candidate for applications that require larger quantities of PAW, such as environmental remediation, industrial disinfection, and agricultural irrigation.

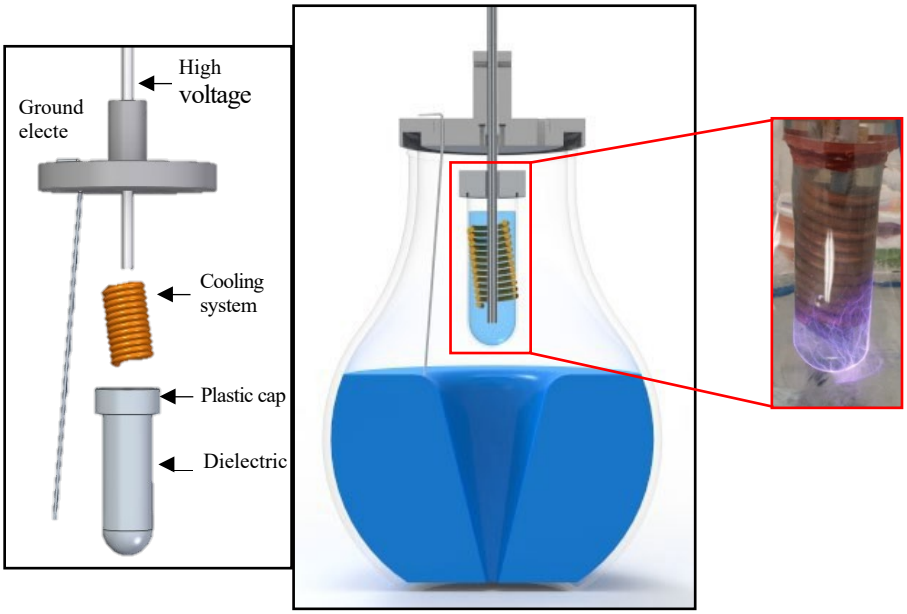

Fig.3: DBD source for 2 l treatment of PAW

3.3 Comparison of corona discharge and DBD CAP Sources.

Despite the higher discharge power of the DBD source (138.60 ± 10.6 W) compared to the corona source (79.47 ± 3.6 W), the larger treated volume (2 l) results in a lower energy density of 0.0250 kW/L compared to the corona source at 0.0260 kW/l (Fig. 4). Additionally, the reduction in energy density is associated with an increase in RONS concentration, as shown in Figures 2 and 5. The efficiency of RONS production,

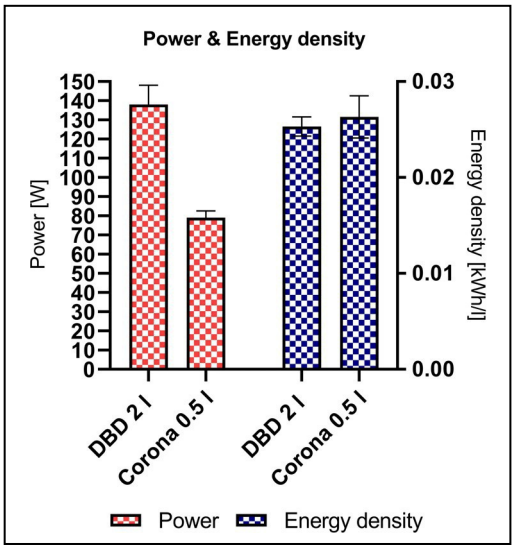

Fig. 4: Discharge power and energy density.

calculated based on hydrogen peroxide, nitrite, and nitrate concentration in distilled water, was 0.34 and 0.25 mol/kWh for DBD and corona, respectively.

3.4 PAW and Plasma Activated Phosphate Buffered Saline solution (PABS): characterization and dental application.

This section reports the effects of cold atmospheric plasma treatments on distilled water and phosphate- buffered saline (PBS), focusing on the electrical and chemical properties of the PAW generated by these treatments. Furthermore, we will explore the application of PAW in dental treatments, particularly the modulation of dentinal enzymatic activity, which is crucial for the longevity of dental restorations.

3.4.1 Electrical and chemical characterization of PAW.

The voltage (V) and current (I) were measured using a high-voltage probe (TEKTRONIX P6015A) mounted on the high-voltage cable and a current probe (TEKTRONIX TCP0030) mounted on the ground cable. Both probes were connected to a digital oscilloscope (TEKTRONIX MSO46). The average power (P) dissipated in the discharge was determined using the following formula:

$$P = \frac{1}{T}\int_0^T V(t)I(t)\,dt$$

Where T is the period of the applied voltage. The average power over a period was calculated based on the current and voltage measurements. The acquired voltage and current values were processed using a Matlab code to calculate the average discharge power consumed by the sources. Matlab was also used to calculate the standard deviation and generate voltage and current waveform graphs. Various tests were conducted to identify the optimal operating conditions of the DBD source for maximizing reactive species concentrations in PAW. The DBD plasma source was a micro-pulsed (AlmaPulse, AlmaPlasma s.r.l) generator set at a fixed frequency of 12 kHz; this system produces plasma in the air gap between the DBD glass tip and the liquid surface. The peak voltage monitored with the voltage probe was 17,5 kV and 17,4 for distilled water and PBS, respectively (Fig. 5). The

water, grounded through a stainless-steel cylinder, is continuously stirred at 750 rpm to ensure uniform treatment. Two liquids were treated: distilled water (DW) and phosphate-buffered saline (PBS). The treatment time was 22 minutes. The electrical analysis showed distinct voltage and current waveforms for each liquid. The average discharge power was measured at 138.60 ± 10.6 W for distilled water and 154.32 ± 10.3 for PBS.

The untreated distilled water and PBS pH values were 5,83 and 7,34, respectively. After the treatment, 25 ml of PAW was collected in a calibrated container for each sample. Additionally, the pH and conductivity of untreated water were measured; the pH was measured using a pH meter (inoLab® pH 7110), while conductivity was measured with a conductometer (Oakton Instrument: Con 6+ Meter).

The concentration of RONS was initially determined semi-quantitatively using QUANTOFIX analytic strips of H_2O_2, NO_2^-, and NO_3^-. Quantitative measurements of H_2O_2, NO_2^-, and NO_3^- were subsequently carried out using the Amplex Red Hydrogen Peroxide Assay Kit (Thermo Fisher Scientific #A22188) and the Nitrite/Nitrate Colorimetric Assay Kit (ROCHE #11746081001), respectively. The Amplex Red molecule, in the presence of the HRP (Horse Radish Peroxidase) catalyst, reacts with H_2O_2 to form water and resorufin. To determine the concentration of NO_2^- and NO_3^-, the Griess reaction was used. This two-step reaction results in the formation of a diazo dye.

The sample was placed in a cuvette, which was then inserted into a plate reader (Microplate reader RT-2100C, Rayto China), where a light beam with wavelength λ was directed at the cuvette. The intensity of the outgoing radiation (I) was lower than the intensity of the incoming radiation (I_0), as shown in Fig. 9a. The Amplex Red Hydrogen Peroxide Assay and Nitrite/Nitrate Colorimetric Assay kits quantitatively determine the concentrations (n) of reactive species by using Lambert-Beer's law. The law can be expressed as:

$$n = -\frac{1}{L\sigma}\ln\left(\frac{I(\lambda)}{I_0(\lambda)}\right)$$

where L is the optical path length, σ is the absorption cross-section, and λ is the wavelength that maximizes the cross-section. For this law to be applicable, the molecule of interest must absorb light at a specific wavelength. The absorbance (A) measured by the spectrophotometer is defined as:

$$\mathrm{A} = -\ln(\mathrm{T})$$

where T is the transmittance, which is the ratio between the outgoing and incoming radiation intensity. By introducing e, the inverse of the absorption cross-section, a linear relationship between absorbance and concentration can be established:

$$A = e\,L\,c$$

where L is the optical path (in cm), c is the concentration (in mol/l), and absorbance is dimensionless. When a certain concentration level is exceeded, this linearity is no longer observed (as shown in Fig. 9b). Both resorufin and the diazo dye puct can absorb light at 570 nm, allowing for the quantification of H_2O_2, NO_2^-, and NO_3^- concentrations.

The analyzed RONS concentration and pH values were:

- DW; H_2O_2: 9.63 ± 0.07 mg/l, NO_2^-: 19.11 ± 1.20 mg/l, NO_3^-: 375.70 ± 7.2 mg/l, pH: 3.42 ± 0.24 (Fig. 6),
- Phosphate-Buffered Saline (PBS): H_2O_2: 9.71 ± 0.20 mg/l, NO_2^-: 36.1 ± 0.83 mg/l, NO_3^-: 505.72 ± 15.26 mg/l, pH: 7.11 ± 0.1 (Fig. 6).

These results show that both liquids generated similar concentrations of hydrogen peroxide (H_2O_2), but PBS demonstrated significantly higher levels of nitrites (NO_2^-) and nitrates (NO_3^-). The difference in pH values—acidic for distilled water and neutral for PBS—likely contributed to

the variance in RONS production. The composition of PBS, which includes buffering ions, may enhance the generation and stability of certain reactive nitrogen species. Notably, peroxynitrous acid, which forms under acidic conditions from hydrogen peroxide and nitrite, is unlikely to be present in PBS due to its neutral pH[2].

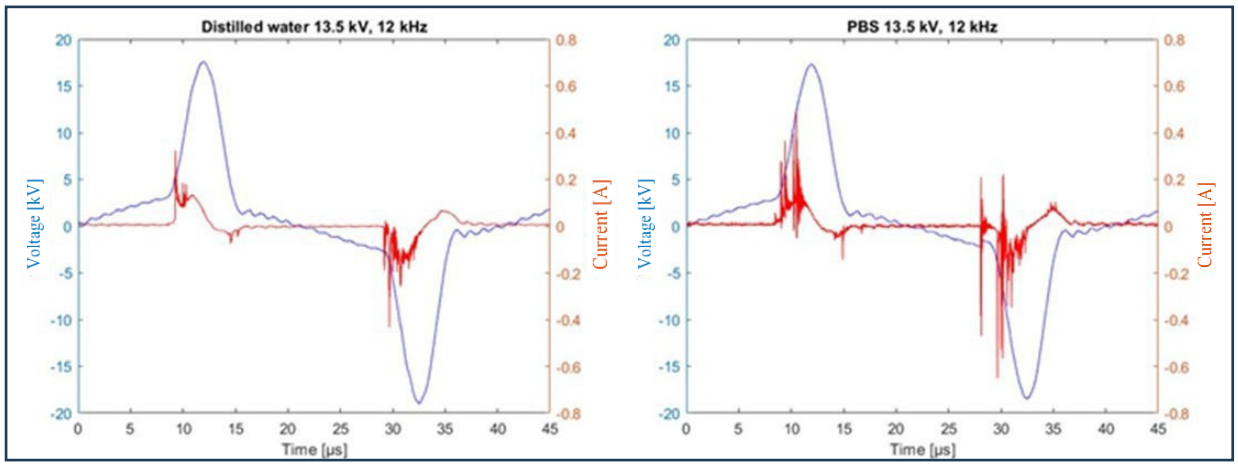

Fig. 5: Voltage and current waveforms for Distilled water and PBS treatment.

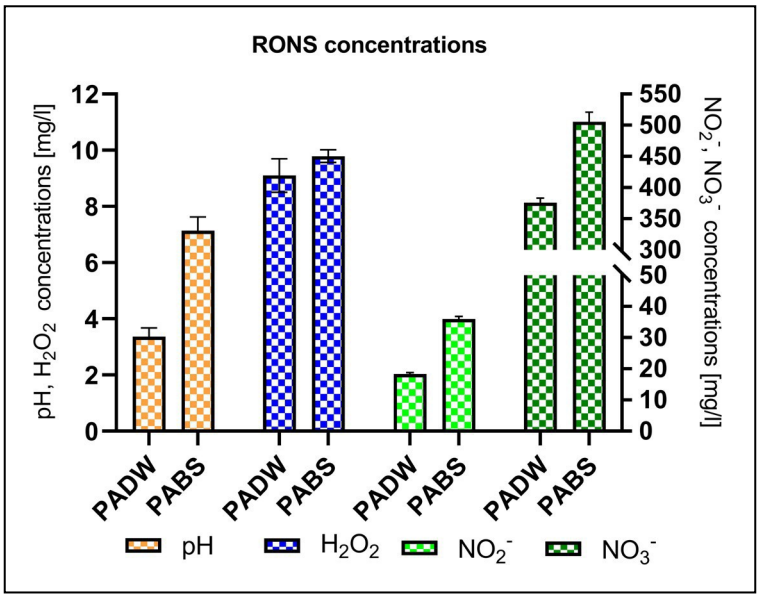

Fig.6: RONS concentration and pH values of PADW and PABS.

3.4.2 Application of plasma activated liquids in dentistry.

PAW offers significant advantages in dental applications because of its antimicrobial and anti-inflammatory properties, making it an ideal candidate for disinfection and regeneration in restorative dentistry [3]. In this study, we specifically examined the effects of plasma activated distilled water (PADW) and plasma activated PBS (PAPBS) on dentinal matrix metalloproteinases (MMPs). These enzymes play a critical role in the degradation of the resin-dentin interface, impacting the longevity of adhesive dental restorations.

3.4.3 Influence of PAW on MMPs activity.

These results were reported to show the full, complete picture of the effects of the DBD source I developed. Experiments on the activation of PAW and PABS were performed in the Golgi BioPlasma Cell laboratory in the Industrial Engineering Department (DIN) of the University of Bologna. In contrast, the experiment on the influence of PAW and PABS on metalloproteinases (MMPs) activity was performed at the Department of Biomedical and Neuromotor Sciences thanks to the collaboration of Doctor Tatjana Maravic from Alma Mater Studiorum University of Bologna. Paper to be submitted: “Influence of various plasma-activated liquids on dentin's intrinsic enzymatic activity” Tatjana Maravic, Roberto Montalbetti, Tijana Lainovic, Claudia Mazzitelli, Diego D’Urso, Vittorio Checchi, Lorenzo Breschi, Romolo Laurita, Matteo Gherardi. Journal: Plasma Medicine, Begell.

MMPs, particularly MMP- and MMP-9, are involved in the breakdown of the collagen matrix within dentin. This enzymatic activity is a significant factor in the hydrolytic degradation of resin-dentin bonds, leading to the eventual failure of composite dental restorations. In this context, controlling or inhibiting MMP activity is crucial for extending the lifespan of adhesive restorations.

Using in situ zymography techniques, we analyzed the effects of PADW and PAPBS on MMP activity in dentin samples. Distilled water and PBS, both in their plasma-activated and non-activated forms, were applied to dentin samples to evaluate how plasma treatment influenced enzymatic activity.

The results showed that PADW increased MMP activity in dentin, while PAPBS reduced it ($p < 0.05$). Non-activated PBS initially exhibited higher MMP activity than non-activated DW, likely because of the presence of ions and the neutral pH of PBS, creating more favorable conditions for enzyme activation. However, the situation changed after plasma activation: the RONS generated in the plasma-activated PBS appeared to inhibit MMP activity. Specifically, the elevated concentration of nitrites and nitrates in PAPBS likely played a role in this inhibition, as previous studies suggest that these reactive nitrogen species can cause structural damage to proteins, including collagen and possibly MMPs. In contrast, DW activation led to increased MMP activity, possibly because of the introduction of hydrogen peroxide through plasma treatment. H_2O_2 has been shown to activate MMPs in other contexts, such as dental bleaching agents.

3.4.4 Potential mechanisms and implications for dentistry.

The differences in MMP activation between PADW and PAPBS may be attributed to their differing chemical compositions post-treatment. The acidic pH of PADW, the neutral pH of PAPBS, and the varying concentrations of RONS suggest that these factors play crucial roles in modulating enzyme activity. The higher levels of nitrites and nitrates in PAPBS, in particular, appear to inhibit MMPs, potentially offering a protective effect on the resin-dentin interface.

4. Scale-up of CAP system: production of 6 l of PAW.

This chapter discusses the successful scale-up of a cold plasma system, focusing on a corona multi-pin discharge system designed to activate up to 6 liters of water, emphasizing the technical modifications that made this scale-up possible.

The heart of this scale-up process involved two corona discharge sources, each composed of stainless-steel cylinders with tungsten tips strategically positioned 5 mm above the water's surface. The system was optimized by employing a stirrer beneath the plasma sources, facilitating uniform water treatment by rotating at 1500 rpm. This chapter will focus on the technical aspects of these design choices and the implications of this scale-up for the broader application of PAW in agriculture.

4.1 Corona discharge source design and configuration.

The designing and prototyping methodologies were previously described in chapter 3.2. Atthe core of this plasma system are the two corona discharge sources, each consisting of stainless-steel cylinders fitted with 10 mm tungsten tips. The choice of tungsten was critical for its ability to generate stable electric fields and remain stable at high temperatures, facilitating the formation of corona discharge in the air gap above the water surface. The tungsten tips are placed precisely 5 mm above the free surface of the water, an optimal distance for creating the desired plasma-air-water interface. An essential aspect of ensuring the uniform treatment of the 6 liters of water was the incorporation of a mechanical stirrer placed directly beneath the corona discharge sources. This stirrer rotates at 1500 rpm, effectively circulating the water and preventing any localized concentration of reactive species.

4.2 Electrical characterization corona source.

The electrical characterization was conducted with the methodologies previously described in chapter 3.5.1. The multipin corona source is supplied by a micro-pulsed high voltage generator (AlmaPULSE, Alma plasma s.r.l. operating at a fixed frequency of 4 kHz, which was chosen to ensure reliable plasma production. The power supply (Fig. 7 is calibrated to provide 115 W of discharge power to each source, sufficient to maintain a stable plasma discharge without overheating the system or causing instability in the plasma formation. The voltage and current of the system are continuously monitored using a high-voltage probe (Tektronix P6015A and a current probe (Pearson 6585, both connected to a digital oscilloscope (Tektronix DPO4034. These monitoring tools allow for real-time data collection on the electrical characteristics of the plasma system, ensuring that the corona sources operate within the optimal range throughout the treatment time.

4.3 Chemical characterization of corona source.

Following the plasma treatment, the PAW was analyzed to quantify the concentrations of critical reactive species. The primary species of interest were hydrogen peroxide, nitrite and nitrate, which were measured immediately after the treatment. The RONS concentrations contained in PAW after 30 min of plasma treatment were 1.13 ± 0.18 mg/l H_2O_2, 18.29 ± 1.94 mg/l NO_2^- and 78.27± 7.86 mg/l NO_3^- (Fig 1. As expected, a reduction in the concentrations of H_2O_2, NO_2^- was noted reaching a minimum of 0.57 ± 0.003 mg/l and 12.62 ± 0.59 mg/l respectively (Fig 1. Meanwhile, NO_3^- concentration increases after the plasma treatment, reaching the value of 103.70 ± 0.097 mg/l after 2 h. The pH and conductivity of the liquid at the end of the plasma treatment are 3.57 ± 0.49 and 105.63 ± 1.65 µS/cm, respectively (Fig 2, and resulted stable after 2 h. The increase of the concentration of nitrates and the reduction of the concentration of hydrogen peroxide and nitrites, two compounds can be attributed to the well-known process of peroxynitrous acid

formation, which occurs from the reaction between hydrogen peroxide and nitrites [4], also leading to nitrate formation.

4.4 Discussion of the scale-up process.

The successful scale-up of the cold plasma system from 2 to 6 liters demonstrates the feasibility of using corona discharge sources for larger-scale production of plasma-activated water. The key to this scale-up was incorporating two symmetrically positioned corona sources with tungsten tips and a high-speed stirrer to ensure uniform water treatment. The system generated high concentrations of reactive species, including hydrogen peroxide, nitrite, and nitrate, which were dispersed throughout the water volume, thanks to the continuous circulation provided by the stirrer.

This scale-up represents a significant advancement in developing plasma-activated water systems for agricultural use. By successfully scaling up to 6 liters, this system paves the way for further increases in volume and broader application of industrial farm settings. Future research should explore the potential for even larger-scale systems and the implications of PAW use in open-field agriculture.

4.5 Application of CAP technology for agricultural purposes.

This paragraph presents an application of the cold plasma source technology described in the previous (section 4.3. The following article is published in the scientific journal PLOS ONE and focuses on the practical implementation of PAW in agriculture. The study explores the use of PAW generated by the hybrid cold plasma system in enhancing plant growth and pathogen resistance, offering detailed insights into its potential benefits. The work discussed in this chapter builds upon the earlier technical foundation and demonstrates plasma technology's broader implications in modern agricultural practices, and lead to the publication of a Paper: "Enhancement of pharmaceutical drug components production in Catharanthus roseus by LED light and plasma activated water (PAW elicitation" Alessandro Quadri; Alberto Barbaresi; Patrizia

Tassinari; Assunta Bertaccini; Nicoletta Contaldo; Laura Mercolini; Michele Protti; Roberto Montalbetti; Romolo Laurita; Daniele Torreggiani. Journal: Plos One.

These results were reported to show a full picture of the effects of the Corona source I developed. Experiments on the activation of 6 liters of tap water were performed at the Department of Food Science and Technology as an experiment on enhancing alkaloid production in *Catharanthus roseus,* thanks to Doctor Alessandro Quadri.

The development of CAP sources for PAW production occurred in agriculture within a multi-disciplinary collaboration involving agricultural sciences laboratories. My role focused on the technical refinement of plasma systems to enhance the generation of reactive species, which were applied in plant models. These collaborations allowed for an in-depth exploration of how PAW can influence plant resilience and yield. The testing and validation in controlled environments ensured the findings were relevant to practical, large-scale agricultural systems.

4.5.1 Electrical characterization of the coronaSource.

The setup (Fig. 7 allowed for real-time monitoring of the voltage and current waveforms, which provided insights into the plasma discharge behavior and the energy being transferred to the water.

The Corona source was supplied with a micro-pulse (AlmaPULSE, Alma plasma s.r.l. generator with a fixed frequency of 4 kHz.

The peak voltage monitored with the voltage probe was 13.8 kV. The discharge power was determined by integrating the product of the voltage and current over several complete cycles of the discharge. The average power delivered to the system was calculated to be 114.09 ± 5.6 W, which indicates that the plasma source operates in a stable and controlled manner. The mean energy density was 0.0095 kWh/l. The efficiency of RONS production, calculated based on hydrogen peroxide, nitrite, and nitrate concentration in tap water, was 0.22 mol/kWh.

Figure 8 illustrates the typical voltage and current waveforms for two consecutive periods of plasma operation. The nearly sinusoidal nature of the voltage waveform indicates that the plasma discharge is uniform and free from perturbations or instabilities. The current waveform, meanwhile, shows periodic spikes corresponding to the pulsed nature of the plasma discharge, reflecting the energy delivered during each microsecond pulse. Maintaining stable plasma conditions is crucial for ensuring the reproducibility of the PAW produced by this system. Any fluctuations in the discharge power or waveform could lead to variations in the concentrations of reactive species generated in the water, potentially affecting the efficacy of the PAW in subsequent applications.

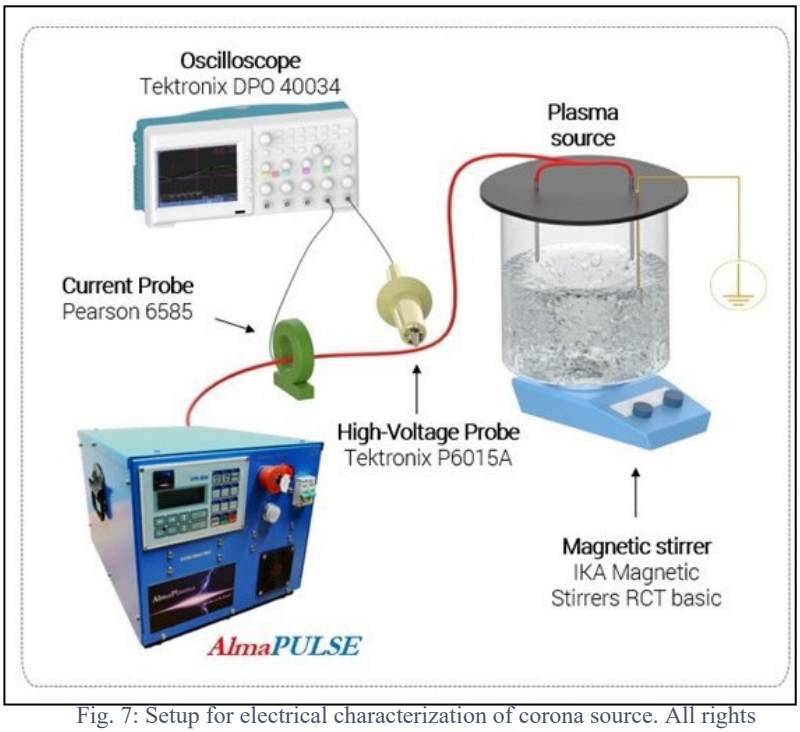

Fig. 7: Setup for electrical characterization of corona source. All rights to this image are owned by [5]

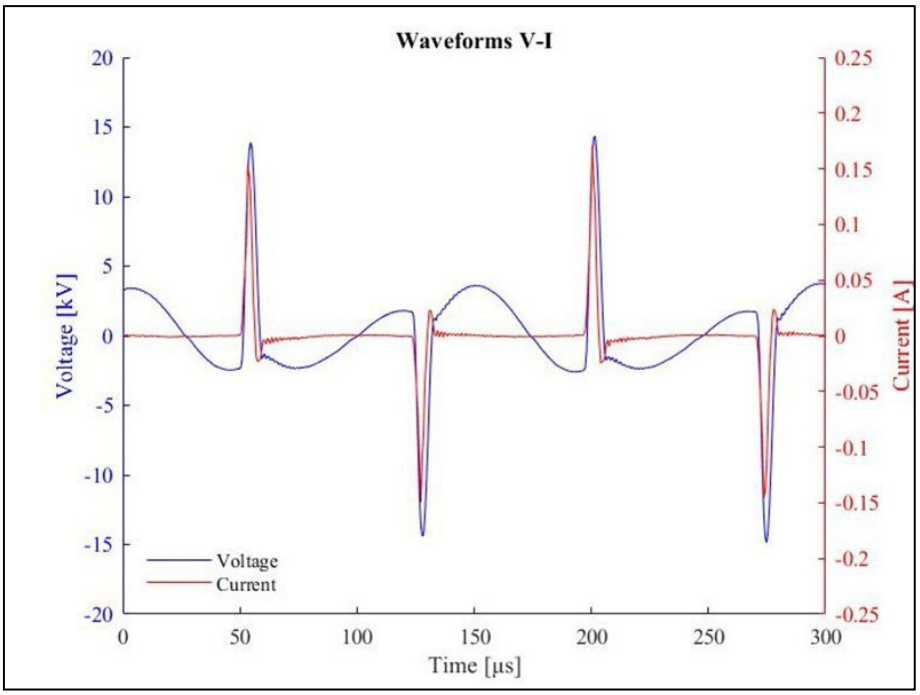

Fig. 8: Current and Voltage waveforms of plasma discharge. All rights to this image are owned by [5]

4.5.2 Chemical characterization of PAW.

The primary reactive species identified in the PAW included hydrogen peroxide, nitrite, and nitrate (Fig. 9a. These species play different roles in plant physiology, with hydrogen peroxide as an oxidative stress signal and nitrite/nitrate as nitrogen sources and signaling molecules. The concentrations of these species were measured immediately after plasma treatment and again one and two hours later to assess the stability of the PAW over time. Immediately after the plasma treatment, the concentration of hydrogen peroxide was measured at 1.13 ± 0.18 mg/l (Fig. 9a. Over the next two hours, this concentration decreased to 0.57 ± 0.003 mg/l (Fig. 9a, likely because of the reaction with nitrite in an acidic environment [4]. This rapid decline in hydrogen peroxide concentration suggests that the PAW should be applied soon after treatment to maximize its biological effects.

As expected, nitrite concentrations followed a similar trend, starting at 18.29 ± 1.94 mg/l and decreasing to 12.62 ± 0.59 mg/l after two hours (Fig. 9a. Nitrite is a key reactive nitrogen species that can participate in various biochemical reactions within plants, including synthesizing secondary metabolites and modulating stress responses [6]. In contrast to hydrogen peroxide and nitrite behavior, nitrate concentrations remained almost stable, with a concentration of 103.70 ± 0.097 mg/l after two hours (Fig. 9a. Nitrate is a stable and bioavailable form of nitrogen that plants can readily absorb and utilize for growth. The increase in nitrate concentration suggests that the PAW retains its effectiveness over time, making it a versatile tool for long-term agricultural applications. Besides the reactive species, plasma treatment also affected the physical properties of the water, including its pH and electrical conductivity. The pH of the water decreased from neutral (6.5 to 3.57 ± 0.49 following plasma treatment because of the formation of acidic species (Fig. 9b. The conductivity of the water increased to 105.63 ± 1.65 μS/cm, reflecting the higher concentration of ions in the solution (Fig. 9b.

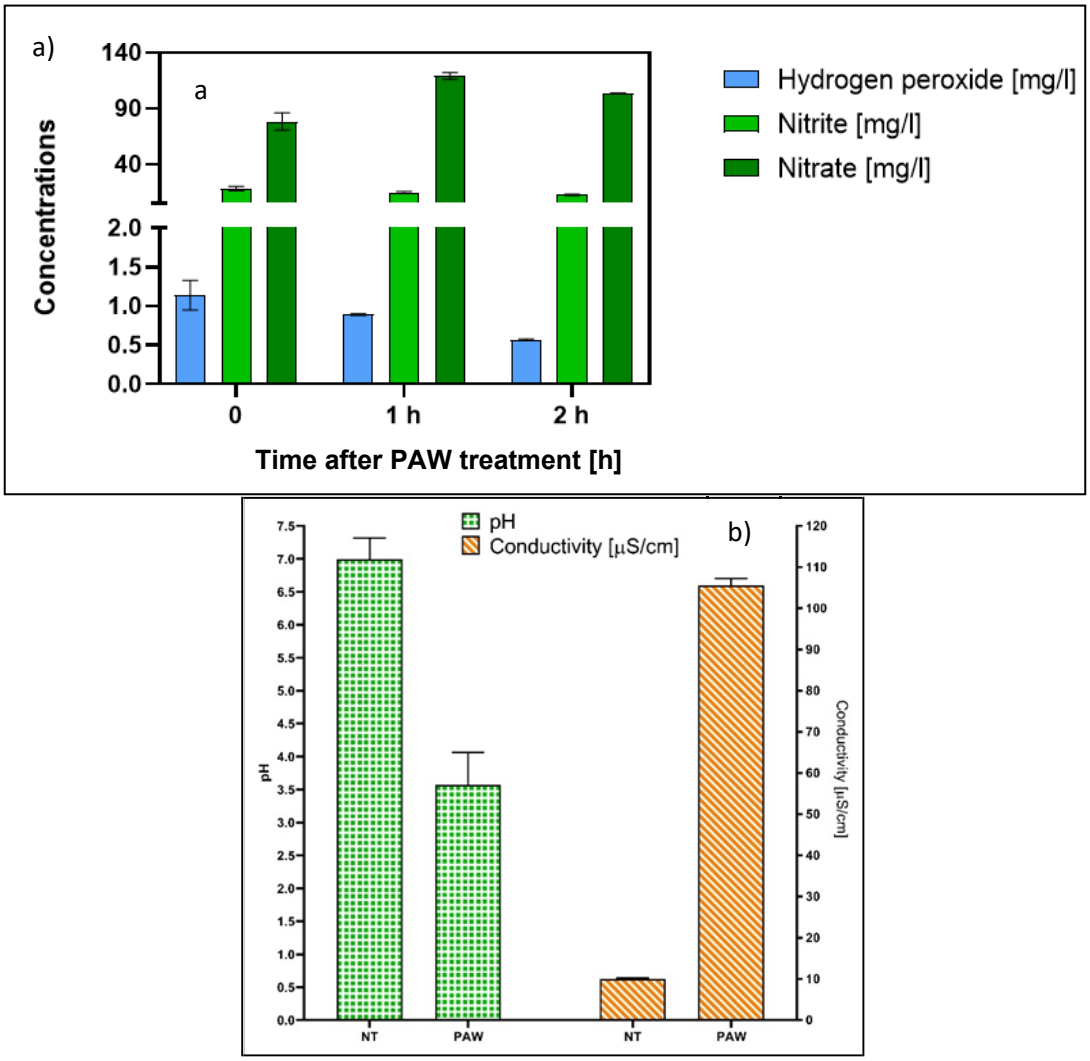

Fig. 9: a) Concentrations of RONS in liquid immediately after the plasma treatment and after 2 hours. b) pH and conductivity of non-treated liquid and PAW. All rights to this image are owned by [5]

4.5.3 Discussion of results and implications.

The results of the electrical and chemical characterization of the plasma source and the PAW it produced provide valuable insights into the mechanisms underlying the generation and efficacy of PAW. The stable plasma discharge, with an average power of 114 W, was effective in producing high concentrations of reactive species in the water, which had a profound impact on the chemical properties of the solution. The observed decrease in hydrogen peroxide and nitrite concentrations

over time highlights the transient nature of these species and the importance of timing in applying PAW. Suppose the PAW is to be used for agricultural purposes. In that case, it should be applied within a short window following plasma treatment to ensure the plants' highest concentrations of reactive species are available. The increase in nitrate concentration over time suggests that PAW could also serve as a slow-release nitrogen source for plants, providing long-term benefits besides its immediate effects. This dual action—both as an immediate elicitor of accentuated responses and a long-term nutrient source—makes PAW a highly versatile tool in plant cultivation.

The scalability of the plasma source used in this study is another important consideration. The relatively low energy consumption of the system (115 W and its modular design make it suitable for both small-scale laboratory experiments and large-scale industrial applications. This scalability is essential for the widespread adoption of PAW in agricultural and environmental applications where large volumes of treated water may be required.

4.5.4 Agricultural applications of PAW.

The application of PAW in agriculture has acquired considerable attention because of its ability to enhance plant growth, stimulate the production of secondary metabolites, and improve plant resistance to environmental stressors [7]. PAW acts as a potent elicitor in plants, leveraging the RONS it contains to initiate biological responses that mirror environmental stress-induced reactions. This makes PAW a valuable tool for increasing plant resilience and promoting the synthesis of secondary metabolites, many of which have high pharmaceutical value [8]. This study applied PAW to *Catharanthus roseus*, a plant species known for producing valuable alkaloids, including vindoline and catharanthine. These alkaloids are critical precursors in synthesizing the anti-cancer drugs vinblastine and vincristine, making *C. roseus* a vital model organism for studying the effects of PAW [5].

4.5.5 Enhancing secondary metabolite production.

Plants naturally produce secondary metabolites as part of their defense mechanisms. In *C. roseus*, vindoline and catharanthine are essential for producing dimeric alkaloids with potent anti-cancer properties. The challenge lies in increasing the field of these metabolites, as they are usually made in low quantities under normal growing conditions. As demonstrated in this study, PAW can act as a metabolic booster, stimulating the pathways leading to increased alkaloid production.

The experiment showed a significant increase in the concentration of vindoline and catharanthine in plants treated with PAW, particularly when combined with red LED light. The synergistic effect of PAW and red light was most pronounced at the sampling point 70 days after planting, where the concentration of vindoline reached 29.4 μg/g dry weight in plants treated with PAW and red light. This represents a 66% increase compared to plants treated with white light without PAW. This finding is critical because it shows how PAW, in conjunction with optimized light conditions, can lead to a marked improvement in producing valuable compounds in medicinal plants. Given the high demand and market value of alkaloids like vindoline and catharanthine, this enhancement has significant implications for pharmaceutical production and agricultural practices.

4.5.6 Benefits of PAW incontrolled environments.

PAW can be particularly advantageous in controlled environment agriculture (CEA, where plants are grown in highly regulated conditions. The ability to manipulate environmental factors such as light, temperature, and humidity allows for the precise application of PAW at the most effective points in the plant's growth cycle. The results of this study suggest that PAW applications are most effective when paired with red light, which is known to activate critical metabolic pathways in plants. The increased concentrations of catharanthine, reaching 70.4 μg/g dry weight in plants treated with PAW and red light, compared to 33.0 μg/g dry weight in plants treated with white light without PAW, emphasize the role of light spectrum and reactive species in stimulating metabolite production.

The combination of PAW with red light targets the specific wavelengths and chemical conditions that favor the biosynthesis of alkaloids. These findings highlight the potential for using PAW in medicinal plant cultivation and any agricultural system where high-value compounds are produced.

5. Designing a new hybrid CAP Source for enhanced RONS generation.

5.1 Hybrid source design and configuration.

As outlined in the previous chapters (4, the cold plasma system for plasma-activated water production has already been scaled to handle volumes of up to 6 liters. However, the current focus is on further optimizing the system to maximize the production of RONS within this fixed volume of water. This chapter will provide a comprehensive analysis of the new hybrid cold plasma source, followed by a detailed discussion on applying the optimized system in practical agricultural settings. The hybrid plasma source used for PAW production is depicted in Fig. 10. The designing and prototyping methodologies were previously described in chapter 3.2.

Fig. 10a shows the DBD source, consisting of the following components:

- Glass jar containing 6 liters of tap water from the public water supply.
- High-voltage liquid electrode and a ground electrode.
- Glass test tube (dielectric material of the high voltage electrode) containing 100 ml of a conductive aqueous solution.

Fig. 10b illustrates the Corona source, consisting of the same ground electrode and a high-voltage pointed electrode.

The lid of the jar, 3D printed, had holes for accommodating the DBD high-voltage liquid electrode, the Corona source, and the ground electrode. The DBD source comprises a high-voltage electrode immersed in a conductive aqueous solution. The high-voltage electrode is a trapezoidal Tr8 stainless steel threaded screw used to adjust the distance of the source tip from the water surface. Adjusting the distance of the source from the water surface is crucial for increasing or decreasing

the volume of water to be treated and positioning the glass test tube within the vortex created by the magnetic stirrer. This also allows for a 5 mm gap between the test tube and the water to facilitate plasma discharge. The conductive solution in which the high-voltage electrode is immersed is created by saturating the water with NaCl and is contained within a glass test tube (a dielectric material. The glass test tube has a glued cap with two lateral threaded holes, allowing it to be fixed to the high-voltage electrode using M6 hex-head screws. The ground electrode is a 2 mm diameter stainless steel cylinder submerged in the water to be treated for PAW production. The Corona source features a high-voltage electrode (a pointed 10 mm diameter tungsten cylinder positioned 5 mm from the water surface and the same ground electrode used for the DBD source. The high-voltage electrode of the Corona source is fixed to the lid using nuts attached to both lid surfaces.

5.2 Experimental setup for electrical characterization.

The operating conditions for the hybrid source are reported in Table 1. Setting the voltage to 18 kV allowed for the maximization of RONS concentrations dissolved in water, although this resulted in the operation time of the DBD being set to 45 s in excessive heating of the conductive aqueous solution and the glass test tube. To resolve this issue, the operation time of the DBD was alternated with that of the Corona source so that the 300 s operation of the latter allowed the DBD to cool down. These treatments, with the DBD operating for 45 s at 18 kV – 4 kHz and the Corona operating for 300 s at 9 kV – 4 kHz, was repeated 6 times to achieve a total treatment time of 270 s for the DBD and 1800 s for the Corona source. After the treatment (with the sources turned off, the magnetic stirrer was operated for 3 minutes to ensure proper mixing.

	Voltage [kV]	**Frequency** [kHz]	**Treatment time** [s]
DBD Rod	18	4	45
Corona	9	4	300

Table 1: Final Operating Conditions for DBD- and Corona Sources

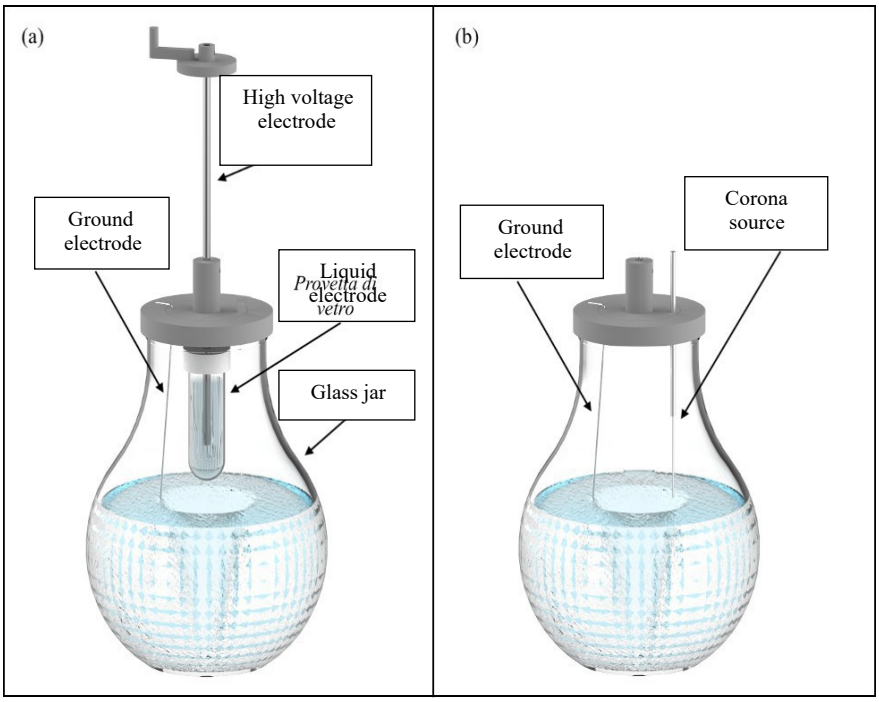

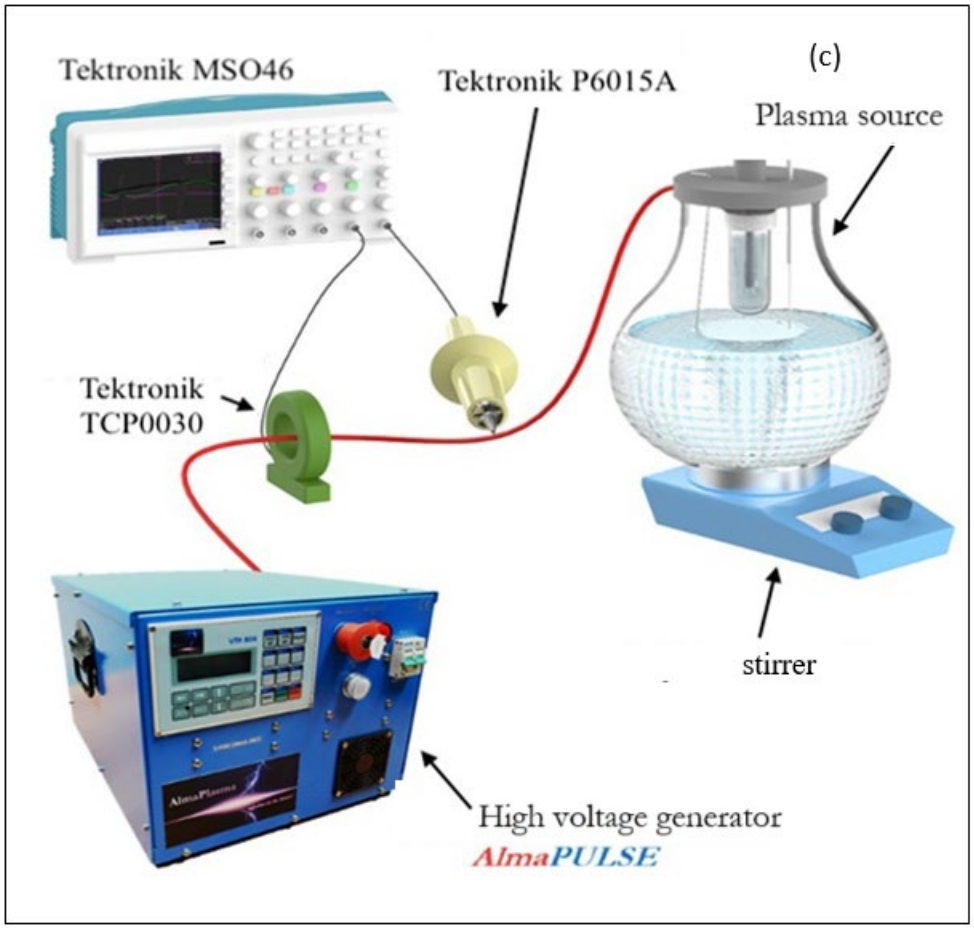

Fig. 10: Hybrid plasma source. a) DBD- source. b) Corona source. c) Setup for Electrical Characterization.

5.3 Electrical characterization.

The electrical characterization was conducted with the methodologies previously described in chapter 3.4.1. The electrical characterization was performed under the following operating conditions:

- DBD: 18 kV voltage, 4 kHz frequency, 270 s total treatment time, and the liquid electrode was filled with 100 ml aqueous conductive solution.
- Corona source: 9 kV voltage, 4 kHz frequency, and 1800 s total treatment time.

The mean discharge power values of the CAP sources are shown in Fig. 13. Under these operating conditions (18 kV-4 kHz), the voltage and current waveforms for the DBD source are shown in Fig. 11 while the voltage and current waveforms for the Corona source under 9 kV and 4 kHz operating conditions are shown in Fig. 12. The peak voltage monitored with the voltage probe was 23,50 kV and 2,30 kV for DBD and Corona respectively. For the DBD, the average discharge power is 250.37 ± 29.3 W, and for the Corona source, it is 82.21 ± 12.1 W (Fig. 15). The mean density energy of the hybrid source was 0.01 kWh/l. The efficiency of RONS production, calculated based on hydrogen peroxide, nitrite, and nitrate concentration, was 0.92 mol/kWh.

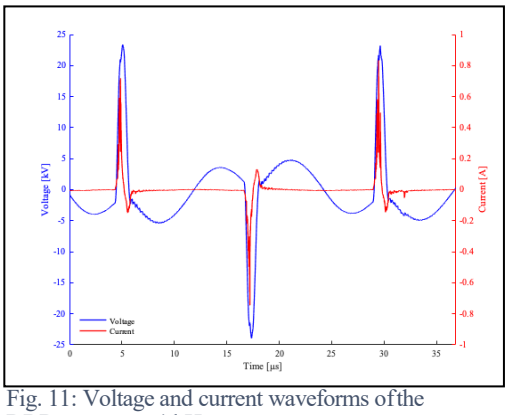

Fig. 11: Voltage and current waveforms of the DBD source at 4 kHz.

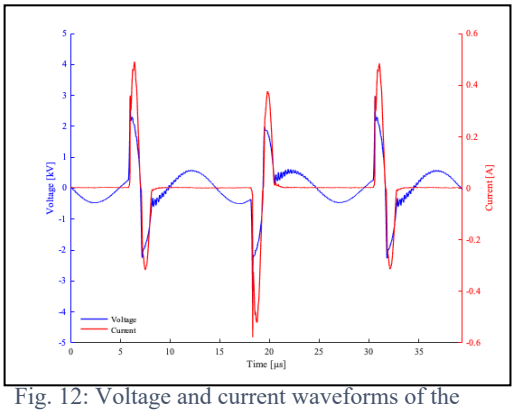

Fig. 12: Voltage and current waveforms of the Corona source at 4 kHz.

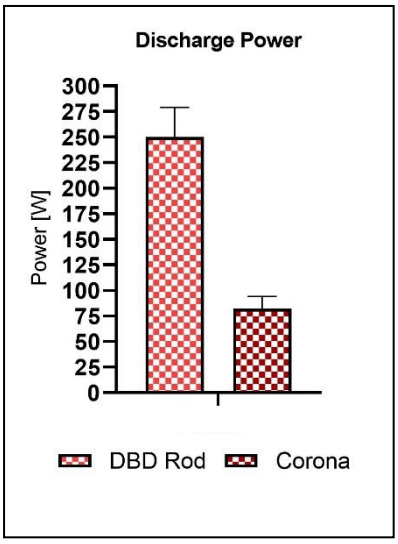

Fig. 13: Discharge power.

5.4 Chemical characterization of PAW.

As previously indicated (5.1, PAW was produced by exposing 6 liters of tap water from the public water supply to plasma treatment using both sources (DBD and corona. The quantitative analysis of RONS were conducted with the methodologies previously described in chapter 3.4.1. After treatment, 25 ml of PAW was collected in a calibrated container; for each sample, pH and conductivity were measured. Additionally, the pH and conductivity of untreated water were measured for comparison. The pH was measured using a pH meter (inoLab® pH 7110, while conductivity was measured with a conductometer (Oakton Instrument: Con 6+ Meter.

5.5 Storage Conditions.

After the treatment, PAW was stored under various temperature conditions, in different types of containers, and with varying volumes. The following storage conditions were investigated:

- Temperature: 24 °C, 4 °C, -20 °C, and -80 °C.
- Storage material: plastic (polypropylene - PP) andglass.
- Volume: 5 ml, 10 ml, and 20 ml.

All measurements were taken from PAW produced under the same operating conditions previously used (DBD source: 18 kV, 4 kHz, 45 s treatment time; Corona source: 9 kV, 4 kHz, 300 s treatment time; cycle repeated six times). The concentrations of reactive species were reported after 7 days of storage, and their variations were analyzed by comparing them with measurements taken immediately after treatment.

5.6 Chemical characterization results.

Fig. 14 presents the quantitative results of reactive species concentrations after treatment with both sources under the same operating conditions previously used (DBD source: 18 kV, 4 kHz, 45 s treatment time; Corona source: 9 kV, 4 kHz, 300 s treatment time; cycle repeated six times). The hydrogen peroxide concentrations were 3.2 ± 0.20 mg/l, while the nitrite concentrations were 62.60 ± 7.2 mg/l. The pH and conductivity values of untreated and treated water arepresented in Figures 15 and 16. Figure 20 shows the conductivity measurement of the untreated solution and the solution immediately after treatment with both sources under the final operating conditions mentioned above. No relevant differences in conductivity are observed between the untreated water sample and the PAW.

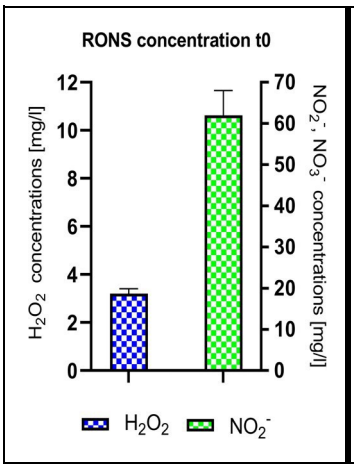

Fig. 14: Quantitative reactive species concentrations at t0.

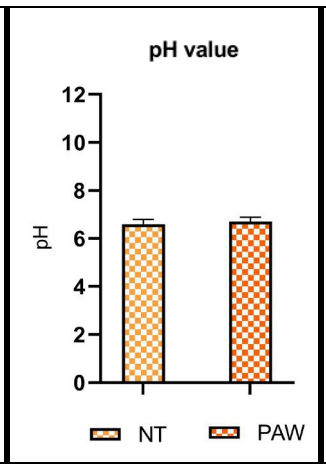

Fig. 15: pH values of Not treated and PAW.

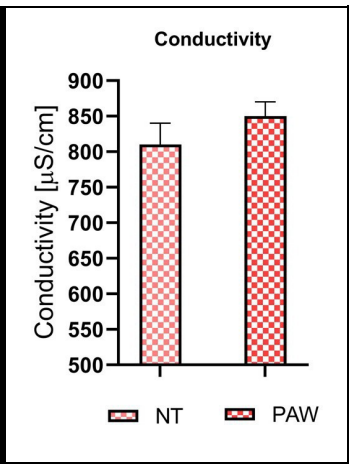

Fig. 16: Conductivity values of Not treated and PAW.

5.7 Delay time effect.

Figures 17 and 18 show the measurements of hydrogen peroxide concentrations after seven days of storage. These figures illustrate the storage results for PAW stored in different containers (glass and plastic and at various temperatures. Specifically, the left side of the graph in Figure 22 refers to the hydrogen peroxide concentrations after storage at 24 °C, while the right side refers to storage at 4 °C. The left side of the graph in Figure 26 refers to hydrogen peroxide concentrations after storage at -20 °C, while the right side refers to storage at -80 °C. The colors representdifferent stored volumes: blue for 5 ml, yellow for 10 ml, and light blue for 20 ml.

The most noticeable characteristic from the comparison between Figures 22 and 23 is the overall decrease in hydrogen peroxide concentration. Additionally, some variability is observed between the different storage conditions. The optimal storage condition is 20 ml in glass at 4 °C, even though better preservation at lower temperatures was expected. The lowest concentration was found at -20 °C. Plastic proved to be a worse material for PAW storage than glass, except at room temperature. Furthermore, the storage volume seems to affect hydrogen peroxide concentration, with higher volumes leading to higher concentrations, except with glass at 24 °C.

Figures 19 and 20 are analogous to the previous ones and refer to nitrite concentrations measured after 7 days of storage in glass and plastic containers under the same temperature and material conditions. Once again, the colors correspond to the different stored volumes: red for 5 ml, violet for 10 ml, and grey for 20 ml.

It is interesting to note that the nitrite concentrations slightly decreased from the values measured at t_0 (~62 mg/l), but no differences are observed between storage at 24 °C and 4 °C.

As with hydrogen peroxide, the worst storage condition for nitrites was at -20 °C, with a concentration of 50 mg/l, regardless of the volume or material. The best storage condition was in glass at 4 °C. Storage at -80 °C in glass is also related to the same output as 4 °C in glass, except for 20 ml volume of storage, where the concentration was the lowest among the analyzed volumes.

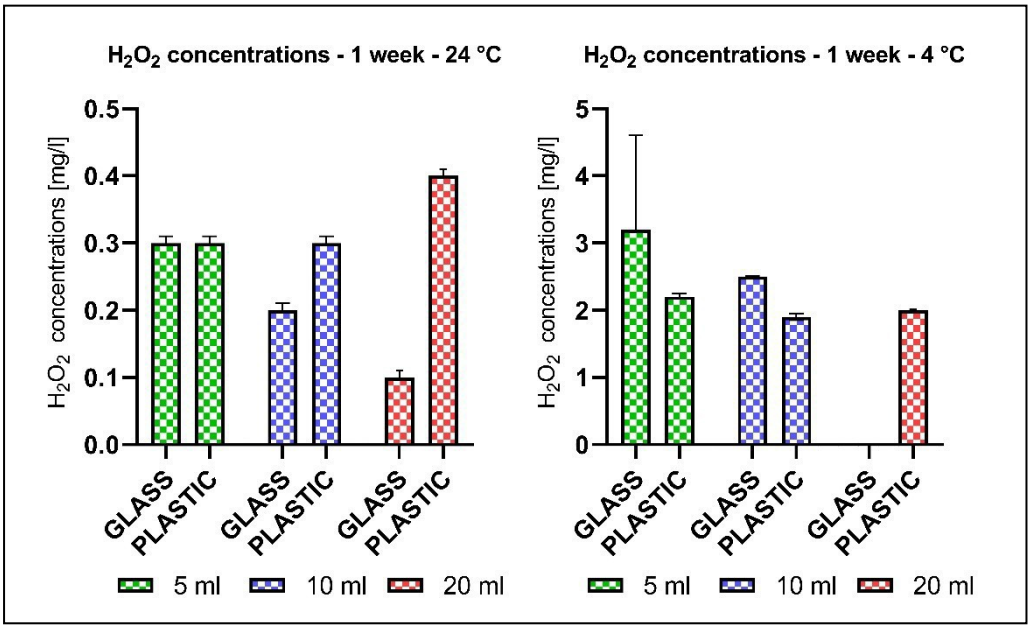

Fig. 17: Hydrogen peroxide concentration after 7 days (PAW stored at 24 °C and 4 °C).

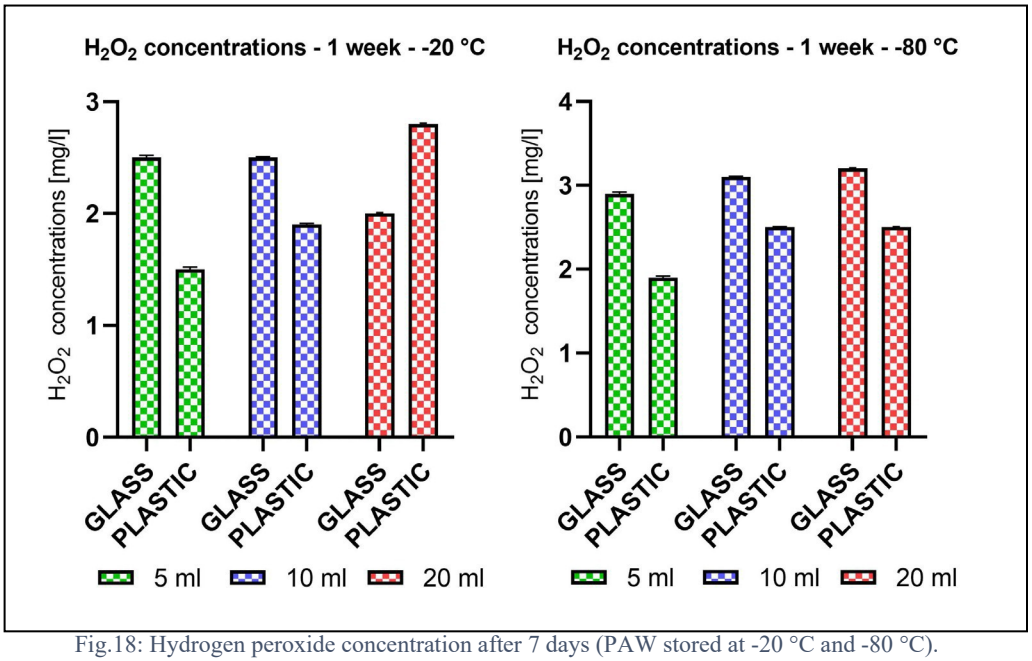

Fig.18: Hydrogen peroxide concentration after 7 days (PAW stored at -20 °C and -80 °C).

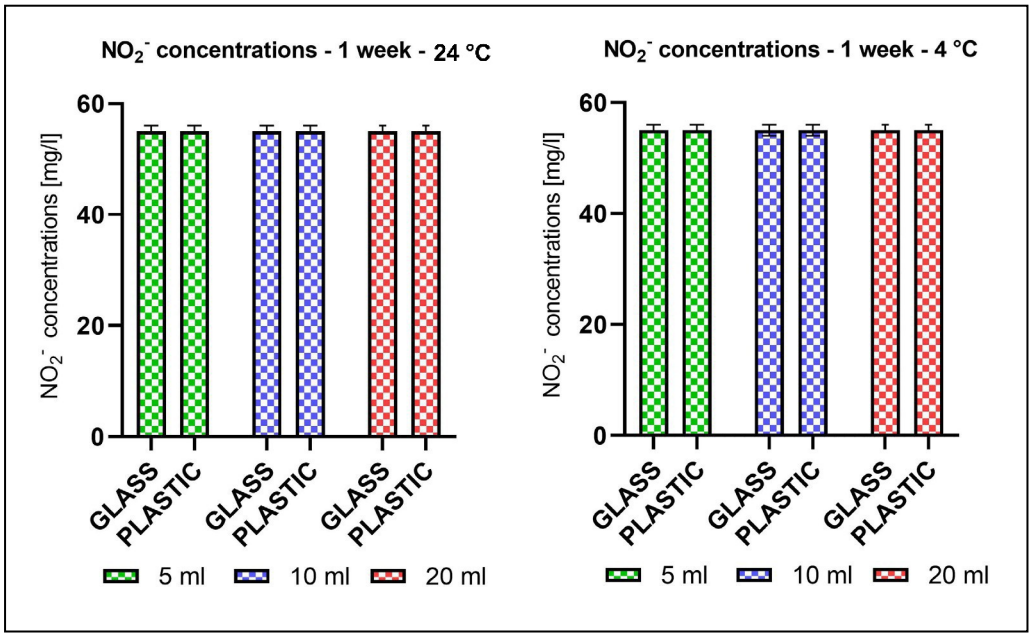

Fig. 19: Nitrite concentration after 7 days (PAW stored at 24 °C and 4 °C).

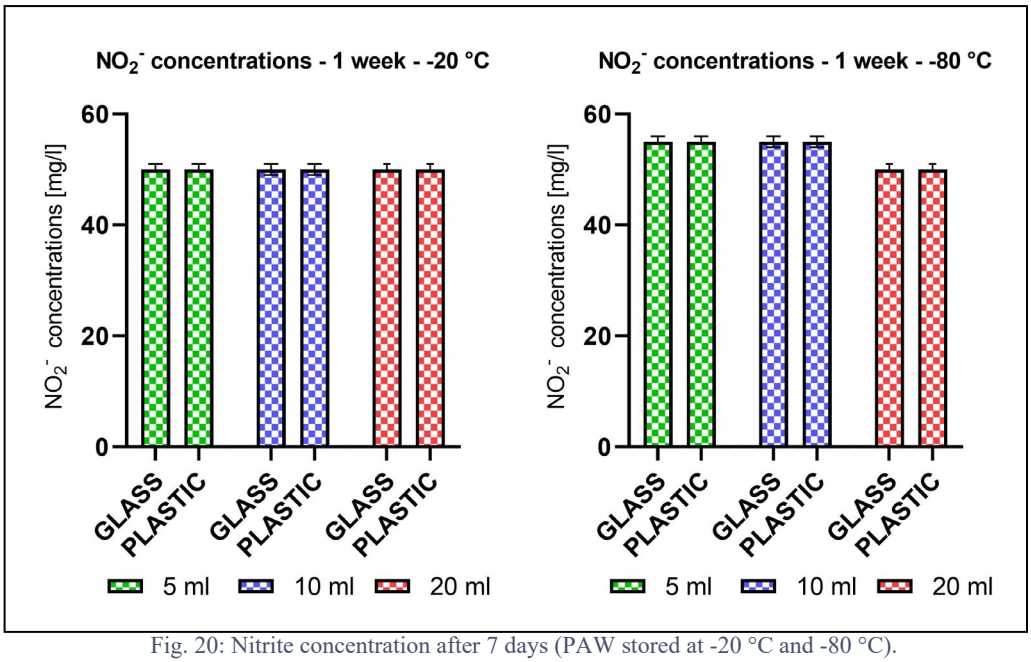

Fig. 20: Nitrite concentration after 7 days (PAW stored at -20 °C and -80 °C).

5.8 Application of the optimized hybrid CAP Source: Practical insights.

With the optimized plasma system in place, the next step was to apply the PAW in agricultural experiments. The primary focus was on evaluating the effects of PAW on the growth and productivity of *Solanum lycopersicum L*. (cv Micro-Tom, a tomato variety commonly used in hydroponic studies because of its compact size and rapid growth cycle. These results were reported to show the full picture of the effects of the Hybrid source I developed. Experiments on the activation of 6 liters of tap water were performed at the Department of Food Science and Technology as an experiment on enhancing alkaloid production in *Solanum lycopersicum L* thanks to Prof. Assunta Bertaccini.

The experiments were designed to assess the impact of the optimized PAW on plant growth, root development, fruit yield, and overall plant health. The treated plants were grown in hydroponic systems, where their roots were immersed in PAW for 30 minutes during two critical periods: 15 days after transplanting (DAT and 42 DAT. These PAW treatments were compared to control groups, which received standard nutrient solutions without PAW. The results were monitored over

the course of the plant's growth cycle, with specific attention given to morphological and physiological traits such as leaf number, stem diameter, plant height, and chlorophyll content. M,

The application of optimized PAW had a profound effect on plant growth. Plants treated with PAW exhibited significantly higher root biomass, with the roots appearing healthier and more robust compared to those of the control plants. This increase in root mass translated to better nutrient uptake, which supported more vigorous above-ground growth. The PAW-treated plants also produced a greater number of leaves and flowers, leading to higher fruit yields at the end of the growth cycle. The fruits themselves were larger and more uniform in size, with improved flavor and color, likely because of the enhanced nutrient absorption facilitated by the optimized PAW.

Chlorophyll content was another key indicator of plant health, and the PAW-treated plants consistently showed higher chlorophyll levels than the control plants. This increase in chlorophyll suggests that the PAW enhanced the plants' photosynthetic capacity, allowing them to convert sunlight into energy more efficiently. The improved photosynthetic activity, combined with the greater root biomass, resulted in faster growth rates and higher overall plant productivity.

Beyond the morphological benefits, the optimized PAW also had a notable effect on the plant's gene expression. Analysis of gene expression data revealed that PAW-treated plants exhibited an upregulation of stress-response genes during the early stages of growth. This molecular response likely contributed to the plants' increased resilience to environmental stressors, such as changes in temperature or humidity. In particular, the expression of phenylalanine ammonia-lyase (PAL), a gene associated with plant defense mechanisms, was significantly higher in the PAW-treated plants during the first 41 days after transplanting. This early activation of defense pathways may have played a role in the plants' improved growth and resistance to disease.

Besides the biological effects observed in the plants, the chemical analysis of the optimized PAW revealed that the concentrations of reactive species remained stable over time. This stability is critical for practical applications, as it ensures that the PAW retains its efficacy even if there is a

delay between its generation and its application in the field. The ability to generate and store PAW for later use could have significant implications for large-scale farming operations, where water treatment systems may need to operate continuously to meet the demands of crop irrigation.

5.9 Conclusion.

This chapter has shown several attempts to optimize the hybrid cold plasma source for the treatment of 6 liters of water, with the specific goal of increasing the concentration of reactive oxygen and nitrogen species (RONS. By optimizing both the electrical aspects of the system, the plasma source could generate significantly higher concentrations of hydrogen peroxide, nitrite, and nitrate in tap water. These improvements were validated through practical experiments, which showed that the optimized PAW had a beneficial effect on plant growth and productivity, particularly during the early stages of development.

6. Conclusion.

This doctoral research advances PAW production by addressing the limitations of scale and efficiency outlined in Chapter 2: Literature Review. Traditional CAP systems, often constrained to a treatment volume of only 0.5 liters, have faced significant efficiency challenges that limit their applicability in industrial contexts. To overcome these limitations, this thesis presents a structured series of scale-ups, each optimizing water treatment volumes, energy densities, and production efficiencies.

The initial phase, described in Chapter 3, utilized a corona discharge setup with a 0.5-liter treatment capacity. Although effective in generating PAW with notable reactive species output, the small treatment volume posed a clear limitation. The energy density for this setup was approximately 0.0260 kWh/l, with a discharge power of 79.47 W and a production efficiency of about 0.25 mol/kWh. This baseline setup demonstrated that while the corona discharge source could achieve efficient PAW production in small volumes, it would require further adaptation for larger-scale applications.

The second phase, introduced in Chapter 4, scaled up to a DBD system capable of treating 2 liters of water. This scale-up involved modifications to the discharge setup, which ensured consistent plasma exposure and energy utilization across a larger water volume. The DBD system maintained an energy density of approximately 0.025 kWh/l, with a discharge power averaging 138.6 W. Production efficiency improved to 0.34 mol/kWh, rendering the DBD setup viable for mid-scale applications by balancing energy demands with effective PAWoutput.

In Chapter 5, the third scale-up involved a dual corona discharge configuration with a capacity of 6 liters. The system incorporated two symmetrical corona sources along with mechanical stirring to ensure a homogeneous RONS distribution across the treated water volume. Each source operated at a discharge power of 115 W, while the energy density was maintained at approximately 0.025 kWh/l. Production efficiency (0.23 mol/kWhmatched that of the DBD system, indicating

that this dual corona discharge setup is suitable for larger treatment capacities without significant increases in energy demand, making it ideal for applications in agriculture and sanitation.

The final phase, detailed in Chapter 6, employed a hybrid cold plasma source. This system, capable of treating 6 liters, integrated a high-voltage electrode and multiple dielectric layers to optimize energy distribution and plasma uniformity. The hybrid source achieved an energy density of approximately 0.0235 kWh/l with a discharge power averaging 250 W for DBD and 80 W for corona, resulting in the highest production efficiency recorded in this research at 0.96 mol/kWh (Table 2). In comparing these configurations, each scale-up demonstrates specific advantages based on the application needs. The initial corona discharge setup was effective at a small scale but lacked the scalability for industrial use. The DBD system provided a balanced solution for mid-scale applications, maintaining efficient energy utilization at 2 liters. The multipin corona discharge setup advanced the volume capacity to 6 liters while preserving energy efficiency, showing it is viable for applications that demand higher volumes. Finally, the hybrid source setup excelled in both scalability and efficiency, marking a significant achievement for potential large-scale PAW applications. In conclusion, this thesis establishes a framework for scalable PAW production, showing that with targeted modifications, CAP systems can meet the demands of various industries. Future research should focus on further optimizing energy density, stabilizing production across larger volumes, and exploring new hybrid CAP configurations. The advancements presented here provide a strong foundation for the continued development of efficient, large-scale PAW systems, essential for industries where high reactivity and scalability are critical. This thesis did not include a life cycle assessment (LCA) of the cold plasma sources studied due to the lack of sufficient data in literature. Although an LCA analysis of cold plasma sources for PAW production is necessary for a complete understanding of these processes, the inhomogeneity and lack of data in the literature does not allow for a complete analysis.

Furthermore, critical data on the operational lifespan of the sources, the frequency of maintenance or replacement of components, and the consumption of resources such as feed gases and their life-cycle impacts would be essential.

Scientific studies on Plasma Activated Water (PAW) typically focus on the chemical characterization of reactive species and the energy efficiency of plasma generation. However, they often neglect fundamental aspects necessary for a comprehensive environmental assessment, including greenhouse gas emissions associated with the entire system and the sustainability of the materials employed. Addressing these omissions would represent a significant advancement in understanding the environmental implications of cold plasma technologies and their potential scalability.

Type of source	Efficiency of RONS production [kWh/l]
Corona 0.5 l	0.24
DBD liquid electrode 2 l	0.34
Corona multipin 6 l	0.22
Hybrid 6 l	0.96

Table 2: Efficiency of RONS production.

Appendix I.

This appendix presents the initial tests conducted on the DBD source with the liquid electrode before its integration into the Hybrid source. It includes the results of the electrical and chemical characterization of the analyzed treatments. Subsequently, the attempts to improve the hybrid source are presented. The modifications to the hybrid source involve both an increase in the delivered discharge power and the introduction of water bubbling systems, along with an evaluation of the effectiveness of the production of RONS of introducing aerosol into the discharge atmosphere.

The operating conditions for the DBD source are reported in Table 3. The DBD source was tested with two different frequencies: 5 kHz and 9 kHz. Three voltage levels were applied for each frequency: 8 kV, 10 kV, and 12 kV. Subsequently, because of excessive heating of the conductive aqueous solution in the glass test tube of the liquid electrode, the volume was increased from 50 ml to 100 ml. This increase in volume allowed the treatment time to be extended from 180 s to 300 s without causing excessive heating of the source during the treatment.

Under the 12 kV voltage and 9 kHz frequency operating conditions for the DBD, combined treatments were performed with the Corona source under 9 kV and 4 kHz operating conditions. The test with the hybrid source was performed with the DBD treatment time set at 300 s, followed by a 900 s treatment with the Corona source. The test was then repeated by reversing the order of source usage (first Corona, then DBD). Following these initial tests, the operating conditions of voltage and frequency were adjusted to maximize discharge power by increasing the voltage to 18 kV and varying the frequency to 4 kHz.

Increasing the voltage to 18 kV allowed for the maximization of RONS concentrations dissolved in water, although this resulted in excessive heating of the conductive aqueous solution and the glass test tube. To resolve this issue, the operation time of the DBD was reduced to 45 s. The

operation of the DBD was alternated with that of the Corona source so that the 300 s operation of the latter allowed the DBD to cool down.

The electrical characterization was conducted with the methodologies previously described in chapter 3.5.1. The electrical characterization of the exclusive DBD source was initially carried out at two frequency values 5 kHz and 9 kHz. Figures 21 and 22 present the discharge power trends corresponding to these two frequencies. For each frequency, three different voltage values (8 kV, 10 kV, and 12 kV) were applied. Subsequently, the treatment time varied from 180 s to 300 s, and the volume of the conductive aqueous solution placed inside the liquid electrode of the DBD source was increased from 50 ml to 100 ml of the conductive aqueous solution placed inside the liquid electrode.

<table>
<tr><th>Voltage [kV]</th><th>Frequency [kHz]</th><th>Treatment time [s]</th><th>Volume of liquid electrode [ml]</th></tr>
<tr><td>8</td><td rowspan="3">5</td><td rowspan="6">180</td><td rowspan="6">50</td></tr>
<tr><td>10</td></tr>
<tr><td>12</td></tr>
<tr><td>8</td><td rowspan="3">9</td></tr>
<tr><td>10</td></tr>
<tr><td>12</td></tr>
<tr><td>8</td><td rowspan="3">5</td><td rowspan="6">300</td><td rowspan="7">100</td></tr>
<tr><td>10</td></tr>
<tr><td>12</td></tr>
<tr><td>8</td><td rowspan="3">9</td></tr>
<tr><td>10</td></tr>
<tr><td>12</td></tr>
<tr><td>18</td><td>4</td><td>45</td></tr>
</table>

Table 3: Operating Conditions for DBD- Source.

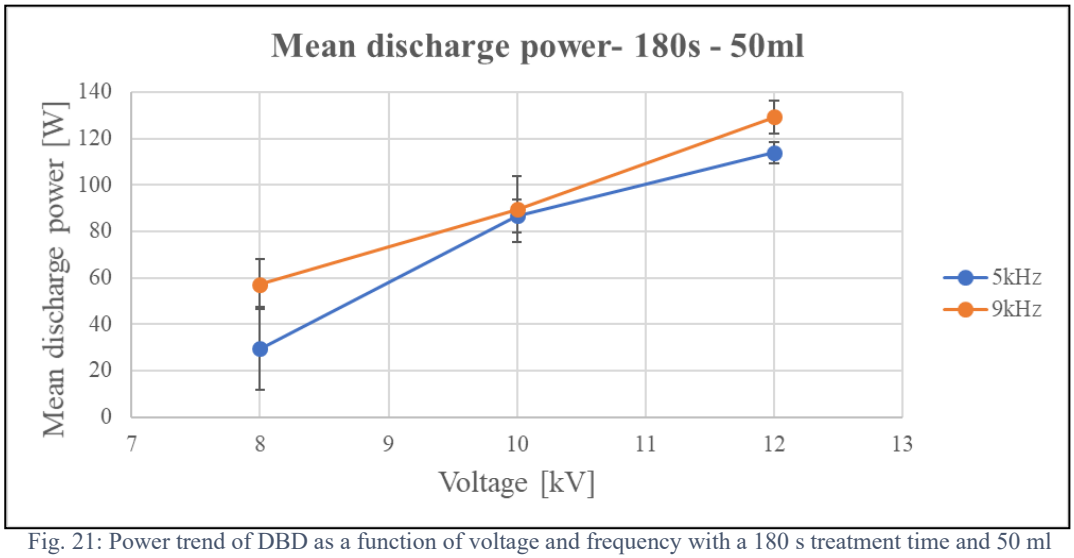

Fig. 21: Power trend of DBD as a function of voltage and frequency with a 180 s treatment time and 50 ml aqueous conductive solution.

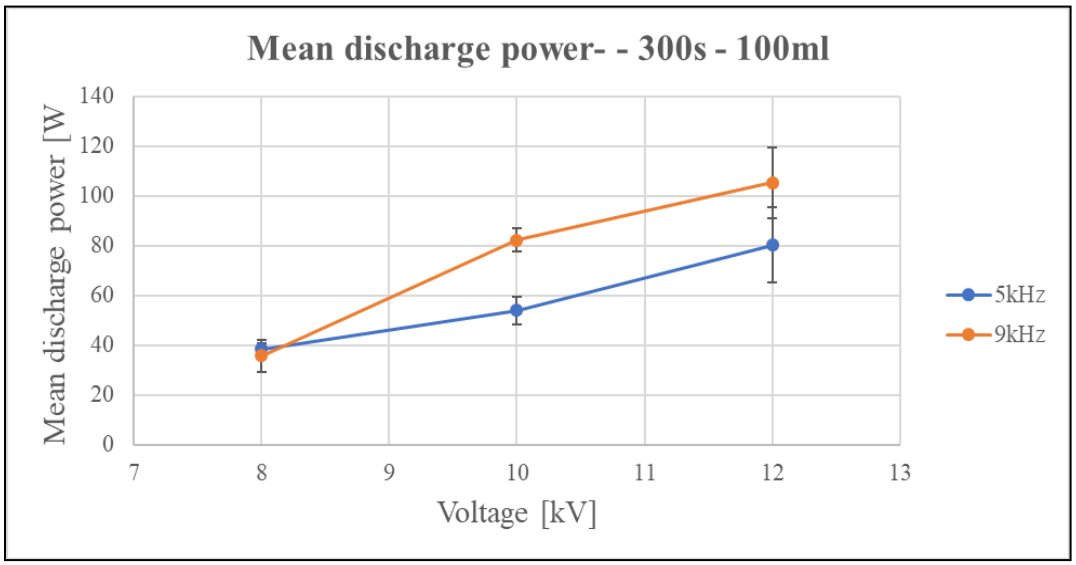

Fig. 22: Power trend of DBD as a function of voltage and frequency with a 300 s treatment time and 100 ml volume of conductive aqueous solution.

Figures 23 and 24 present the concentrations of reactive species measured semi-quantitatively with QUANTOFIX analytics strips after 180 s of an exclusive DBD plasma treatment with 50 ml and 100 ml volume of conductive aqueous solution, varying the frequency (5 kHz and 9 kHz) and voltage (8 kV, 10 kV, 12 kV). It can be observed that the concentrations of reactive species at the two frequencies are similar, and the maximum value is reached with a voltage of 12 kV. As previously mentioned, increasing the applied voltage increases the discharge power, leading to higher concentrations of RONS. The concentration of hydrogen peroxide ranges from 2 to 5 mg/l, nitrate concentration is around 25 mg/l, and nitrite concentration ranges from 0 to 1 mg/l.

Using the DBD source results in a moderate concentration of hydrogen peroxide and nitrates but a low concentration of nitrites.

Increasing the treatment time to 300 s and the volume of the aqueous conductive solution to 100 ml, the reactive species concentrations were again measured semi-quantitatively. Figure 25 shows the concentrations of hydrogen peroxide, nitrate, and nitrite at 5 kHz, with varying voltage (8 kV, 10 kV, 12 kV). Similarly, a lower concentration of reactive species is observed at 8 kV compared to 10 kV and 12 kV. Figure 26 shows the reactive species concentrations at 9 kHz, with a 300 s treatment and 100 ml of conductive solution, while varying the voltage as in the previous case.

From these initial DBD tests, the optimal operating condition that maximized RONS was a treatment time of 300 s, a volume of 100 ml of conductive aqueous solution of the liquid electrode, a frequency of 9 kHz, and a voltage of 12 kV. The concentration of hydrogen peroxide was between 2 to 5 mg/l, nitrate concentration ranged from 25 to 50 mg/l, nitrite concentration was between 0 and 1 mg/l, and hydrogen peroxide was between 2 to 5 mg/l, nitrate concentration ranged from 25 to 50 mg/l, and nitrite concentration was between 0 and 1 mg/l. Subsequently, using the DBD operating at 12 kV – 9 kHz, combined treatments were carried out with the Corona source under the previously selected conditions (9 kV – 4 kHz). First, a 300 s treatment was performed with the DBD, followed by a 900 s treatment with the Corona source. The test was then repeated by reversing the order of source usage (first Corona, then DBD). The results of the reactive species concentrations, evaluated semi-quantitatively with QUANTOFIX analytic strips, are shown in Figure 27. Reversing the order of the two sources reports the same results in terms of reactive species concentrations. In both cases, the concentration of hydrogen peroxide is between 2 to 5 mg/l, nitrate concentration ranges from 250 to 500 mg/l, and nitrite concentration is between 40 and 80 mg/l.

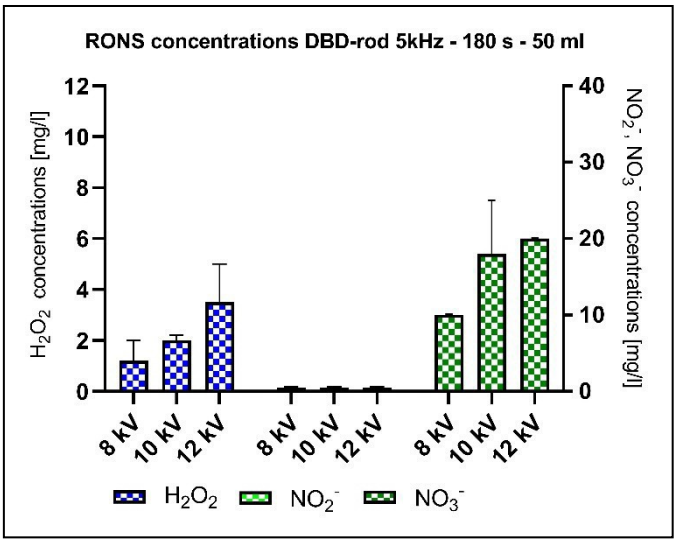

Fig. 23: Hydrogen peroxide concentrations after 180 s with 50 ml of liquid solution for the high voltage liquid electrode of DBD source.

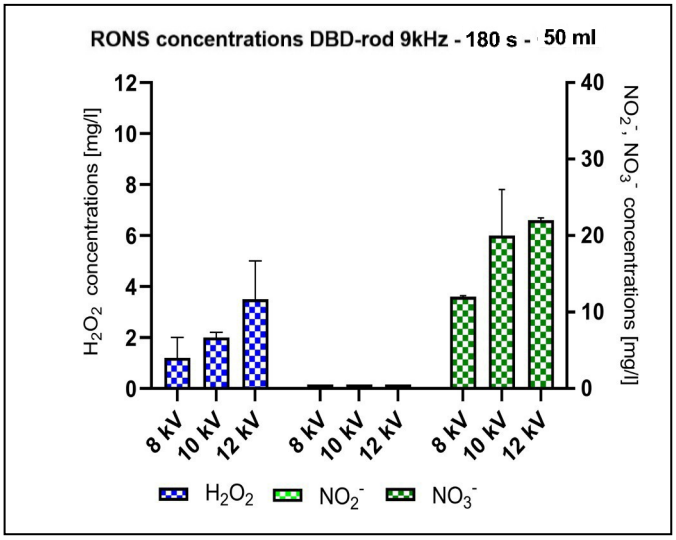

Fig. 24: Hydrogen peroxide concentrations after 180 s with 50 ml of liquid solution for the high voltage liquid electrode of DBD source.

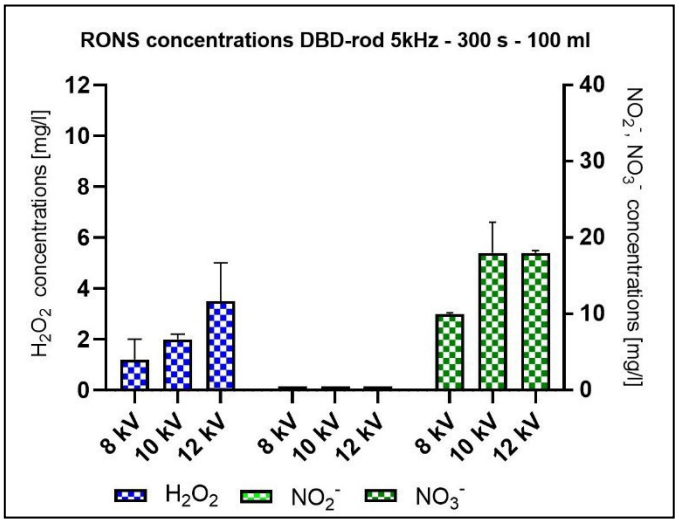

Fig. 25: Hydrogen peroxide concentrations after 300 s with 100 ml of liquid solution for the high voltage liquid electrode of DBD source.

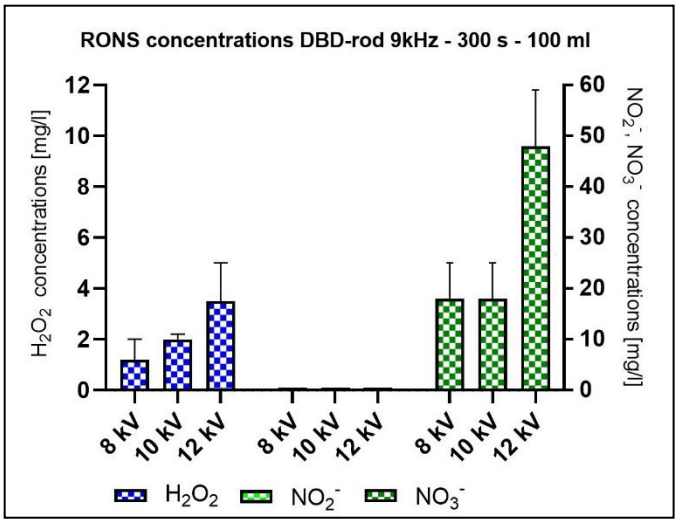

Fig. 26: Hydrogen peroxide concentrations after 300 s with 100 ml of liquid solution for the high voltage liquid electrode of DBD source.

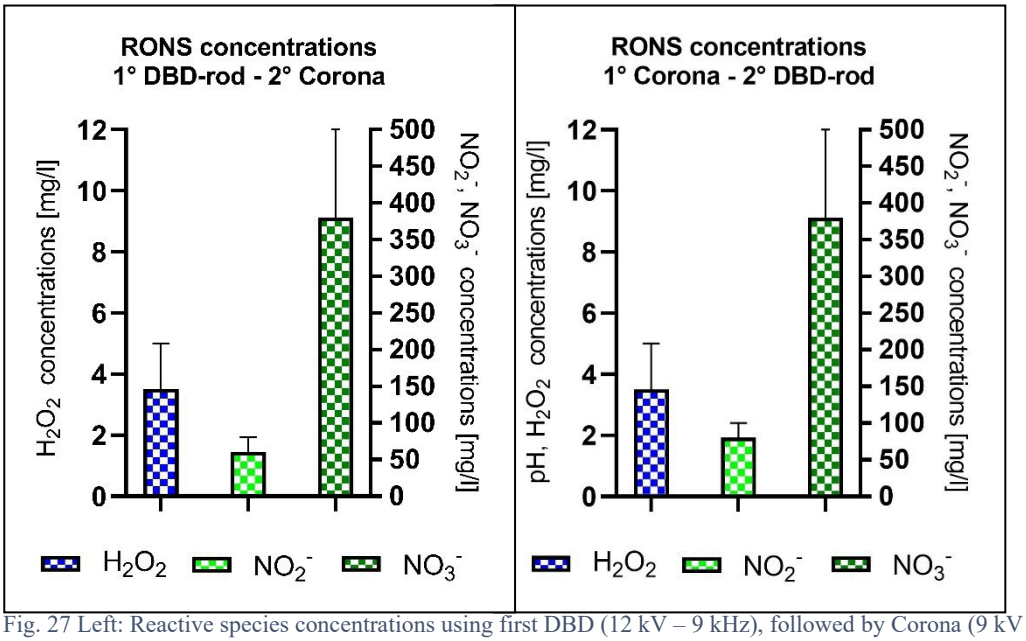

Fig. 27 Left: Reactive species concentrations using first DBD (12 kV – 9 kHz), followed by Corona (9 kV – 4 kHz). Right: Reactive species concentrations using first Corona (9 kV – 4 kHz), followed by DBD (12 kV – 9 kHz).

The most significant issue with the DBD source integrated into the hybrid source was its limited operational lifespan. The thermal stress encountered during treatment caused the conductive aqueous solution placed inside the liquid electrode to boil, exposing the glass container to excessively high temperatures (80-100 °C), which resulted in breakage at the end of each total treatment. This problem was resolved by incorporating a cooling system within the DBD source. The system includes a copper tubing coil positioned inside the glass vial, submerged in the conductive aqueous solution. Distilled water, driven by a submersible pump placed within a 10-liter external reservoir of distilled water, flows through the tubing. The flow rate ensured by the pump was 0.5 l/s. The cooling system effectively extended the service life of the DBD source, eliminating the need to replace the glass container after each cold plasma treatment.

One of the primary factors influencing the generation of RONS in the plasma system is the power discharge of each cold plasma source. The initial configuration of the DBD unit operated at 250 W of discharge power, with a fixed frequency of 4 kHz supplied by a micro-pulsed generator

(AlmaPULSE, Alma plasma s.r.l.). However, to increase the concentration of RONS, the discharge power was raised to 280 W.

The corona discharge unit was similarly optimized. The initial configuration of the Corona unit operated at 80 W of discharge power, with a fixed frequency of 4 kHz supplied by a micro-pulsed generator (AlmaPULSE, Alma plasma s.r.l.). However, to increase the concentration of RONS, the discharge power was raised to 300 W. The electrical characterization was conducted with the methodologies previously described in chapter 3.4.1. The peak voltage monitored with the voltage probe was 17 kV and 11 kV for DBD and corona, respectively (Fig. 28). The discharge power was 275 ± 16.2 W and 294.50 ± 24.9 W for DBD and corona, respectively. The mean density energy of the hybrid source was 0.028 kWh/l. The efficiency of RONS production, calculated based on hydrogen peroxide, nitrite, and nitrate concentration, was 0.50 mol/kWh. To assess the effectiveness of the increased total discharge power of the hybrid source, the treatment liquid was chemically characterized using semi-quantitative methods with QUANTOFIX strips (Fig. 29). The pH was measured using a pH meter (inoLab® pH 7110) (Fig. 30).

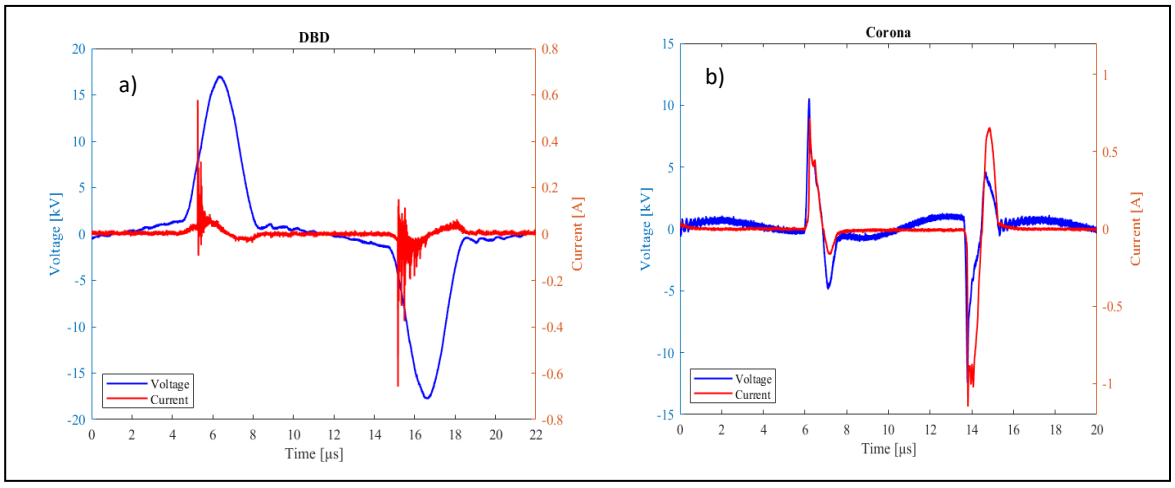

Fig. 28: Voltage and current waveforms for DBD (a) and corona discharge (b), with the optimized electrical conditions.

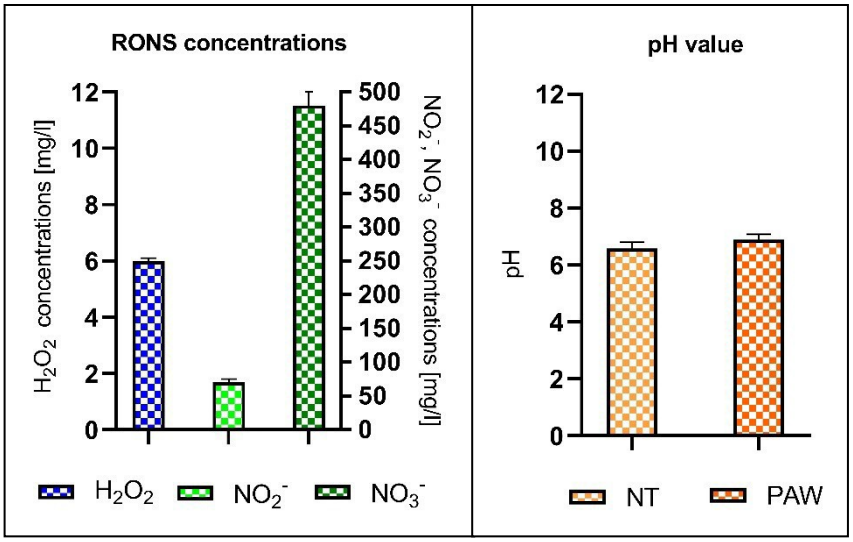

Fig. 29: RONS concentrations with the optimized electrical condition.

Fig. 30: pH values of Not treated water and PAW.

While the electrical optimizations played a critical role in increasing the generation of RONS, the water handling system also had a significant impact on the overall performance of the plasma source. One of the system's critical components was the stirrer, which maintained uniform water movement throughout the 6-liter treatment volume. The stirrer, rotating at 1500 rpm, ensured the water constantly circulated, providing an even distribution of reactive species throughout the entire volume.

Initial tests showed that using the stirrer alone was sufficient to promote uniform plasma-liquid interaction (Chapter 5), but additional modifications were made to enhance the surface contact between water and plasma discharge and the physico-chemical interplay between the liquid and plasma phases. During the early optimization stages, air was bubbled into the system to increase the surface area for plasma interaction. The bubbling system involved a bubbler positioned at the end of a flexible plastic tube with a diameter of 6 mm, connected to a compressed air pump delivering an airflow of 1 m^3/s. The bubbler was positioned in the bottom part of the glass jar where the water to be treated was placed. However, the bubbling system initially used in the plasma chamber was removed after no relevant improvements were analyzed. Still, this method led to a

decrease, compared to one measured without bubbling (Fig. 29), in the concentration of certain reactive species, particularly nitrate (Fig.33).

In response to these findings, the bubbling system was removed entirely, and the stirrer was relied upon exclusively to circulate the water. This change markedly improved the concentration of RONS, particularly hydrogen peroxide and nitrite, as removing bubbles allowed for a more stable and consistent plasma-liquid interface. Using the stirrer ensured that all portions of the water were equally exposed to plasma, preventing localized variations in reactive species concentration.

While removing the bubbling system and using the stirrer significantly improved the performance of the plasma system, additional attempts were made to optimize the interaction between the plasma and the water. Other methods explored involved using aerosol generators designed to create a fine mist inside the plasma chamber. The aerosol system used was derived from medical equipment, filled with 50 ml of tap water, and connected via a flexible plastic tube with a diameter of 6 mm to a compressed air pump delivering an airflow of 1 m^3/s. The aerosol flushed inside the jar through a hole made in the cap of the glass jar where the CAP sources were housed. However, the use of aerosol generators did not yield the expected results. The introduction of the aerosol led to a decrease (Fig. 33) in the concentration of certain reactive species, particularly nitrate, compared to one measured without aerosol (Fig. 29). Additionally, the aerosol particles appeared to interfere with the stability of the plasma, leading to fluctuations in the discharge that reduced the power discharge production of the system. It was determined that the aerosol method was not suitable for this plasma configuration, and the idea was abandoned. Fig. 31 reported the voltage and current waveforms with the bubbling system activated. The hybrid source was supplied with amicro-pulsed generator (AlmaPULSE,Alma plasma s.r.l.) with a fixed frequency of 10 kHz and 3 kHz for DBD and corona, respectively.The peak voltage monitored with the voltage probe was 19 kV and 7.5 kV for DBD and corona respectively with the bubbling system activated. The discharge power with bubbling system activated was 254 ± 8.40 W and 247 ± 18.2 W for DBD and Corona respectively. Fig. 32 reports the voltage and current waveforms with the aerosol system activated

under the same operating conditions described for the bubbling system. The peak voltage monitored with the voltage probe was 19 kV and 2 kV for DBD and corona, respectively, with the aerosol system activated. The discharge power with the aerosol system activated was 269.60 ± 32.5 W and 277.90 ± 23.4 W for DBD and Corona,respectively.

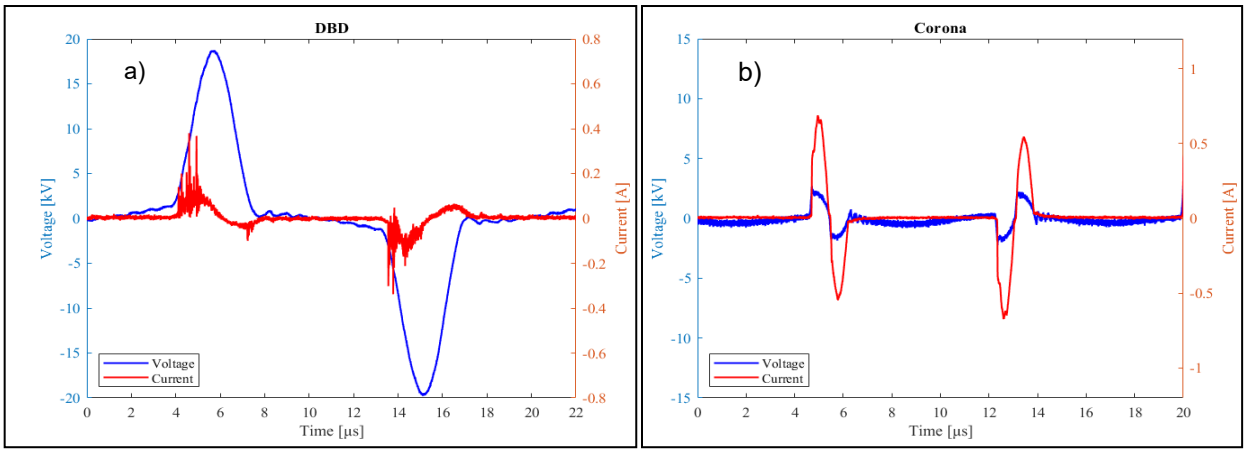

Fig. 31: Voltage and current waveforms for DBD (a) and corona discharge (b), with the bubbling system activated.

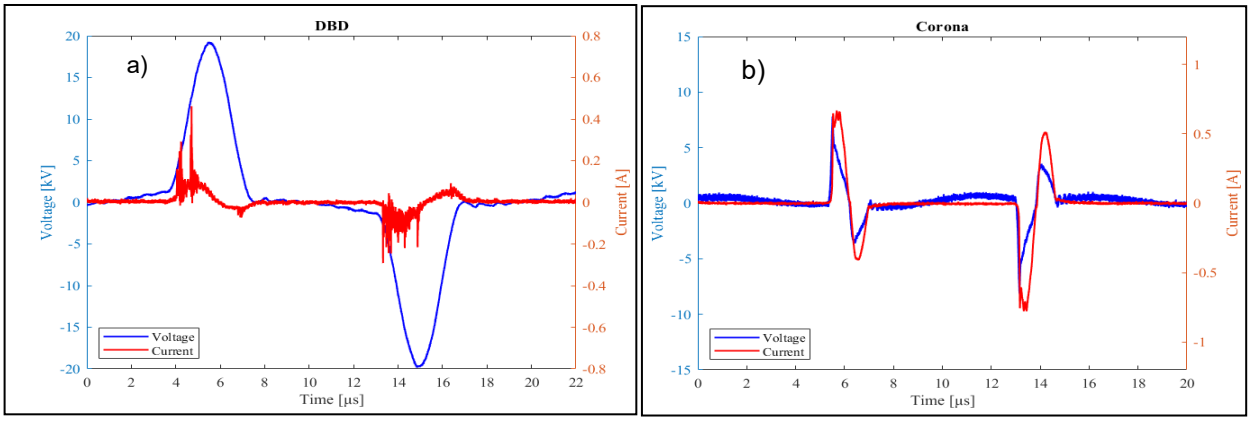

Fig. 32: Voltage and current waveforms for DBD (a) and corona discharge (b), with the aerosol system activated.

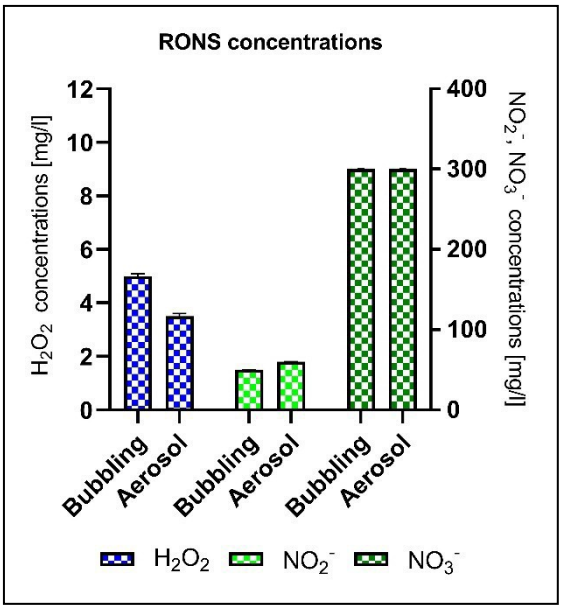

Fig. 33: RONS concentration with bubbling and aerosol system activated separately.

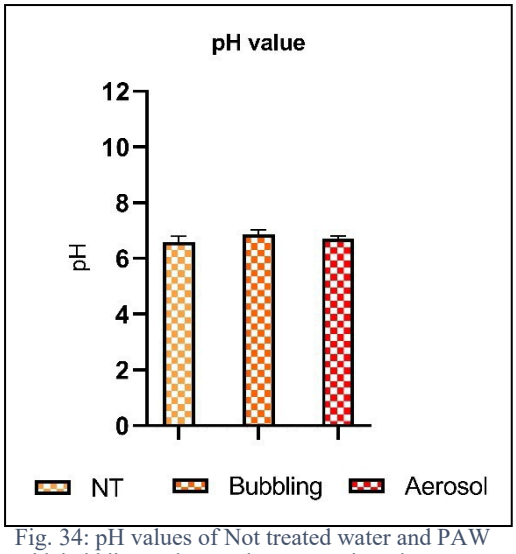

Fig. 34: pH values of Not treated water and PAW with bubbling and aerosol system activated separately.

References.

[1] R Laurita, N Contaldo, Y Zambon, A Bisag, A Canel, M Gherardi, G Laghi, A Bertaccini. *"The use of plasma-activated water in viticulture: Induction of resistance and agronomic performance in greenhouse and open field"*. Plasma Processes and Polymers, 2020, 18, DOI: 10.1002/ppap.202000206.

[2] Girard F, Badets V, Blanc S, Gazeli K, Marlin L, Authier L, Svarnas P, Sojic N, Clément F, Arbault S. *"Formation of reactive nitrogen species including peroxynitrite in physiological buffer exposed to cold atmospheric plasma"*. RSC Adv. 2016, DOI: 10.1039/C6RA12791F.

[3] Noala Vicensoto Moreira Milhan, William Chiappim, Aline da Graça Sampaio, Mariana Raquel da Cruz Vegian, Rodrigo Sávio Pessoa and Cristiane Yumi Koga-Ito. *"Applications of Plasma-Activated Water in Dentistry: A Review"*. International Journal of Molecular Sciences, 2022, 23, 4131, DOI: 10.3390/ijms23084131.

[4] P Lukes, E Dolezalova, I Sisrova and M Clupek. *"Aqueous-phase chemistry and bactericidal effects from an air discharge plasma in contact with water: evidence for the formation of peroxynitrite through a pseudo-second- order post-discharge reaction of H_2O_2 and HNO_2"*. Plasma Sources Science and Technology, 2014, 23 015019.

[5] Quadri, A., Barbaresi, A., Tassinari, P., Bertaccini, A., Contaldo, N., Mercolini, L., Protti, M., Montalbetti, R., Laurita, R., Torreggiani, D. *"Use of LED light and plasma activated water (PAW) to stimulate pharmaceutical compound production in Catharanthus roseus plants"*. Acta Horticulturae, 2024, 19 12, e0315542.

[6] Dingmeng Guo, Hongxia Liu, Lei Zhou, Jinzhuo Xie, and Chi He. *"Plasma-activated water production and its application in agriculture"*. J Sci Food Agric. 2021 Sep;101(12):4891-4899. doi: 10.1002/jsfa.11258. Epub 2021 May 3. PMID: 33860533.

[7] Himani Singh, Niharika, Pradeep Lamichhane, Ravi Gupta, Neha Kaushik, Eun Ha Choi, Nagendra Kumar Kaushik. *"Enhancing crop health and sustainability: exploring the potential of secondary metabolites and non-thermal plasma treatment as alternatives to pesticides"*. Plant Biotechnol Rep 17, 803–820 (2023). https://doi.org/10.1007/s11816-023-00883-0.

[8] Karma Yeshi, Darren Crayn, Edita Ritmejeryt, and Phurpa Wangchuk. *"Plant Secondary Metabolites Produced in Response to Abiotic Stresses as Potential Application in Pharmaceutical Product Development"*.Molecules. 2022 Jan 5;27(1):313. doi: 10.3390/molecules27010313. PMID: 35011546; PMCID: PMC8746929.